ELSEVIER

Journal of Power Sources 110 (2002) 445–470

JOURNAL OF POWER SOURCES

www.elsevier.com/locate/jpowsour

Calendar- and cycle-life studies of advanced technology development program generation 1 lithium-ion batteries

R.B. Wright[a,*], C.G. Motloch[a], J.R. Belt[a], J.P. Christophersen[a], C.D. Ho[a], R.A. Richardson[a], I. Bloom[b], S.A. Jones[b], V.S. Battaglia[b], G.L. Henriksen[b], T. Unkelhaeuser[c], D. Ingersoll[c], H.L. Case[c], S.A. Rogers[d], R.A. Sutula[d]

[a]*Idaho National Engineering and Environmental Laboratory, P.O. Box 1625, MS-3830, Idaho Falls, ID 83415-3830, USA*
[b]*Argonne National Laboratory, 9700 South Cass Avenue, Argonne, IL 60439, USA*
[c]*Sandia National Laboratory, P.O. Box 5800, Albuquerque, NM 87185-0613, USA*
[d]*US Department of Energy, 1000 Independence Avenue SW, Washington, DC 20858, USA*

Abstract

This paper presents the test results and life modeling of special calendar- and cycle-life tests conducted on 18650-size generation 1 (Gen 1) lithium-ion battery cells (nominal capacity of 0.9 Ah; 3.0–4.1 V rating) developed to establish a baseline chemistry and performance for the Department of Energy sponsored advanced technology development (ATD) program. Electrical performance testing was conducted at the Argonne National Laboratory (ANL), Sandia National Laboratory (SNL) and the Idaho National Engineering and Environmental Laboratory (INEEL).

As part of the electrical performance testing, a new calendar-life test protocol was used. The test consisted of a once per day discharge and charge pulse designed to have minimal impact on the cell yet establish its performance over a period of time such that the calendar-life of the cell could be determined. The calendar-life test matrix included two states-of-charge (SOCs) (i.e. 60 and 80%) and four test temperatures (40, 50, 60 and 70 °C). Discharge and regen resistances were calculated from the test data. Results indicate that both the discharge and regen resistances increased non-linearly as a function of the test time. The magnitude of the resistances depended on the temperature and SOC at which the test was conducted. Both resistances had a non-linear increase with respect to time at test temperature. The discharge resistances are greater than the regen resistances at all of the test temperatures of 40, 50, 60 and 70 °C. For both the discharge and regen resistances, generally the higher the test temperature, the lower the resistance.

The measured resistances were then used to develop an empirical model that was used to predict the calendar-life of the cells. This model accounted for the time, temperature and SOC of the batteries during the calendar-life test. The functional form of the model is given by: $R(t, T, \mathrm{SOC}) = A(T, \mathrm{SOC})F(t) + B(T, \mathrm{SOC})$, where t is the time at test temperature, T the test temperature and SOC the SOC of the cell at the start of the test. $A(T, \mathrm{SOC})$ and $B(T, \mathrm{SOC})$ are assumed to be functions of the temperature and SOC; F is assumed to only be a function of the time at test temperature. Using curve-fitting techniques for a number of time-dependent functions, it was found that both the discharge and regen resistances were best correlated with $F(t)$ having a square-root of test time dependence. These results led to the relationship for the discharge and regen resistances: $R(t, T, \mathrm{SOC}) = A(T, \mathrm{SOC})t^{1/2} + B(T, \mathrm{SOC})$. The square-root of time dependence can be accounted for by either a one-dimensional diffusion type of mechanism, presumably of the lithium-ions or by a parabolic growth mechanism for the growth of a thin-film solid electrolyte interface (SEI) layer on the anode and/or cathode. The temperature dependence of the resistance was then investigated using various model fits to the functions $A(T, \mathrm{SOC})$ and $B(T, \mathrm{SOC})$. The results of this exercise lead to a functional form for the temperature dependence of the fitting functions having an Arrhenius-like form: $A(T, \mathrm{SOC}) = a(\mathrm{SOC})\{\exp[b(\mathrm{SOC})/T]\}$ and $B(T, \mathrm{SOC}) = c(\mathrm{SOC})\{\exp[d(\mathrm{SOC})/T]\}$, where a and c are constants, and b and d are related to activation energy (E_b and E_d) by using the gas constant (R) such that $b = E_b/R$ and $d = E_d/R$. The functional form, therefore, for the discharge and regen resistances, including the SOC, is then: $R(t, T, \mathrm{SOC}) = a(\mathrm{SOC})\{\exp[b(\mathrm{SOC})/T]\}t^{1/2} + c(\mathrm{SOC})\{\exp[d(\mathrm{SOC})/T]\}$. The a, b, c and d parameters are explicitly shown as being functions of the SOC. However, due to the lack of testing at SOC values other than 60 and 80% SOC, the exact form of the SOC dependence could not be determined from the experimental data. The values of a, b, c and d were determined, thus permitting the function $R(t, T, \mathrm{SOC})$ to be used to correlate the discharge and regen data and to predict what the resistances would be at different test times and temperatures.

This paper also presents, discusses and models the results of a special cycle-life test conducted for a period of time at specified temperatures of 40, 50, 60 and 70 °C. This test, consisting of specified discharge and charge protocols, was designed to establish the cycle-life performance of the cells over a time interval such that their cycle-life could be determined. The cycle-life test was conducted at 60% SOC, with SOC swings of Δ3, Δ6 and Δ9%. During the cycle-life test, the discharge and regen resistances were determined after every 100 test cycles. The results of

* Corresponding author. Tel.: +1-208-526-0959; fax: +1-208-526-0969.
E-mail address: rbw2@inel.gov (R.B. Wright).

0378-7753/02/$ – see front matter. Published by Elsevier Science B.V.
PII: S0378-7753(02)00210-0

the cycle-life testing indicate that both the discharge and regen resistances increased non-linearly as a function of the test time at each Δ% SOC test. The magnitude of the resistances and the rate at which they changed depended on the temperature and Δ% SOC at which the test was conducted. Both resistances had a non-linear increase with respect to time at test temperature, i.e. as the number of test cycles increased the discharge and regen resistances increased also. For a given Δ% SOC test, the discharge resistances are greater than the regen resistances at all of the test temperatures of 40, 50, 60 and 70 °C. For both the discharge and regen resistances, generally the higher the test temperature, the lower the resistance. At each of the four test temperatures, the magnitude of the discharge and regen resistances was generally in the following order: Δ3% SOC > Δ9% SOC > Δ6% SOC, but the ordering was dependent on test time.

A model was also developed to account for the time, temperature, SOC and Δ% SOC of the batteries during the cycle-life test. The functional form of the model is given by $R(t, T, \mathrm{SOC}, \Delta\%\,\mathrm{SOC}) = A(T, \mathrm{SOC}, \Delta\%\,\mathrm{SOC})F(t) + B(T, \mathrm{SOC}, \Delta\%\,\mathrm{SOC})$ where t is the time at test temperature, T the test temperature, SOC the SOC of the cell at the start and end of the test and Δ% SOC the SOC swing during the test. $A(T, \mathrm{SOC}, \Delta\%\,\mathrm{SOC})$ and $B(T, \mathrm{SOC}, \Delta\%\,\mathrm{SOC})$ are assumed to be functions of the test temperature, SOC and Δ% SOC swing. $F(t)$ is assumed to only be a function of the test time at test temperature. Using curve-fitting techniques for a number of time-dependent functions, it was found that both the discharge and regen resistances were best correlated by a square-root of test time dependence. These results led to the relationship for the discharge and regen resistances having the form $R(t, T, \mathrm{SOC}, \Delta\%\,\mathrm{SOC}) = A(T, \mathrm{SOC}, \Delta\%\,\mathrm{SOC})t^{1/2} + B(T, \mathrm{SOC}, \Delta\%\,\mathrm{SOC})$. This model is essentially the same as used to analyze the calendar-life test data. The temperature dependence of the resistance was then investigated using various model fits to the functions $A(T)$ and $B(T)$. The results of this exercise lead to a functional form for the functions having again an Arrhenius-like form: $A(T) = a[\exp(b/T)]$ and $B(T) = c[\exp(d/T)]$ where a and c are constants, and b and d are related to activation energies. The functional form, therefore, for the discharge and regen resistances including the SOC and Δ% SOC is $R(t, T, \mathrm{SOC}, \Delta\%\,\mathrm{SOC}) = a(\mathrm{SOC}, \Delta\%\,\mathrm{SOC})\{\exp[b(\mathrm{SOC}, \Delta\%\,\mathrm{SOC})/T]\}t^{1/2} + c(\mathrm{SOC}, \Delta\%\,\mathrm{SOC})\{\exp[d(\mathrm{SOC}, \Delta\%\,\mathrm{SOC})/T]\}$. The a, b, c and d parameters are explicitly shown as being functions of the SOC and the Δ% SOC. However, due to the lack of testing at SOC values other than 60% SOC, the exact form of the SOC dependence could not be determined from the experimental data. In addition, no model was found that consistently correlated the observed resistance changes with the Δ% SOC of the tests. Eliminating the SOC and Δ% SOC from the resistance function, the function $R(t, T)$ was then used to correlate the discharge and regen resistances data. This model also allows the prediction of what the resistances would be at different test times at a particular Δ% SOC test condition and temperature.
Published by Elsevier Science B.V.

Keywords: Lithium-ion batteries; Battery calendar-life; Battery cycle-life; Battery modeling; Arrhenius kinetics

1. Introduction

The DOE Office of Advanced Automotive Technologies (OAAT), through the partnership for a new generation of vehicles (PNGV) advanced technology development (ATD) program, is engaged in the study of 18650-size lithium-ion cells to investigate the physical/chemical mechanisms causing performance degradation over the life of these batteries. Concentrating on high-power battery development, the ATD program supports the PNGV, a government-industry partnership striving to develop, by 2004, a mid-size passenger vehicle capable of achieving up to three times the fuel economy of today's vehicles, while adhering to future emissions standards and maintaining affordability, performance, safety and comfort. The ATD program addresses these technical challenges through five major program areas: (1) baseline cell development; (2) diagnostic evaluations; (3) electrochemical improvements; (4) advanced materials development; and (5) low-cost packaging. The major objective of the work is to determine the causes of power fade after the ATD program designed cells are exposed to elevated temperatures and tested under various electrical performance evaluation tests. Another objective is to develop diagnostic analysis methods that can be used to determine the physical/chemical causes for cell degradation.

This paper presents the electrical performance of the generation 1 (Gen 1) lithium-ion cells developed by the ATD program [1] during special calendar- and cycle-life testing conducted at various temperatures and state-of-charge (SOC) [2]. All tests were conducted either in the Energy Storage Testing (EST) Laboratory, which is part of the Transportation Technologies and Infrastructure Department at the Idaho National Engineering and Environmental Laboratory (INEEL), at the Lithium Battery R&D Department 1521 at Sandia National Laboratory (SNL) and at the electrochemical energy technology program at Argonne National Laboratory (ANL).

One of the main points of this paper is to present, discuss and model the calendar-life test data on the lithium-ion batteries developed by the ATD program. Calendar-life is of great importance as one of the PNGV goals is to develop battery systems having a lifetime of 15 years if they are to be a viable energy storage/source for the next generation of vehicles. Calendar-life has been defined by two general statements. The USABC Electric Vehicles Battery Test Procedures Manual, Revision 2 [3] defines calendar-life as "the length of time a battery can undergo some defined operation before failing to meet its specified end-of-life criteria." This definition is rather nebulous. The specific definition of some defined operation would need to be clarified and stipulated in the test plan for a given battery system. The PNGV Battery Test Manual, Revision 2 [4], is also rather terse in its definition of calendar-life: "this test is designed to permit the evaluation of cell degradation as a result of the passage of time with minimal usage. It is not a pure shelf-life test, because the cells under test are periodically subjected to reference discharges to determine the changes (if any) in their performance characteristics."

The ATD program [1] has attempted to more clearly define what is meant by a calendar-life test. The calendar-life test as used in the ATD program has been designed to have a minimal impact on the cell, yet still subject the cell to a well-specified charge/discharge test sequence over a well-defined period of time.

The other topic of this paper is to present, analyze and model cycle-life test data on the cells developed by the ATD program. Cycle-life is also of great importance, as battery systems are expected to have a lifetime of 15 years. Two general statements have defined cycle-life. The USABC Electric Vehicles Battery Test Procedures Manual, Revision 2 [3] defines cycle-life as "the number of cycles, each to a specified discharge and charge termination criteria, such as depth-of-discharge (DOD), under a specified charge and discharge regime, that a battery can undergo before failing to meet its specified end-of-life criteria." This definition clearly depends on the specifics of the test protocols as specified in the test plan for a given battery system. The PNGV Battery Test Manual, Revision 2 (and 3), discusses various cycle-life tests that may be used when testing batteries [4]. The cycle-life test as used in the ATD program has been designed and specified as applicable to the Gen 1 cells developed for this program.

Discussion of the terminology used in this report can be found in [3], USABC Electric Vehicle Battery Test Procedures Manual, Revision 2 and in [4], PNGV Battery Test Manual, Revision 2 (and 3). The entire test procedure used to test the ATD Gen 1 cells is not reproduced herein as much as it is given in [2], PNGV Test Plan for ATD 18650 Gen 1 Lithium-Ion Cells.

The results presented in this paper are more extensively presented in two INEEL reports [5,6]. A paper concerning the rates of the area-specific impedance increase and power fade resulting from the accelerated calendar- and cycle-life tests of the ATD Gen 1 cells has also been published [7].

2. Experimental

2.1. Description of ATD program Gen 1 lithium-ion batteries

The baseline lithium-ion cells had the following specifications, as developed by ANL for the ATD program. Cells produced with these specified materials are referred too as Gen 1 cells.

Positive electrode (cathode) (copper current collector)
$LiNi_{0.8}Co_{0.2}O_2$ (Sumitomo) (84 wt.%)
Electronic additive: acetylene black (4 wt.%) + SFG-6 graphite (Timcal) (4 wt.%)
Binder: polyvinylidene fluoride $(-CH_2-CF_2-)_n$, (PVDF) (Kureha KF-1100) (8 wt.%)

Negative electrode (anode) (aluminum current collector)
Blend of MCMB-6-2800 graphite (Osaka gas) (75 wt.%) and SFG-6 (Timcal) (16 wt.%)
Binder: PVDF (Kureha C) (9 wt.%)

Electrolyte
1 M $LiPF_6$/ethylene carbonate (EC) (1 wt.%) + diethyl carbonate (DEC) (1 wt.%)

Separator
Polyethylene (PE) Celgard separator (37 μm thick)

Three hundred cells were assembled (18650-size; 64.9 mm high, 18.12 mm diameter) and shipped to various national laboratories [ANL, Brookhaven National Laboratory (BNL), INEEL, Lawrence Berkeley National Laboratory (LBNL) and SNL] for electrical performance testing and physical/chemical diagnostic analysis. The cell distribution is given in the test plan [2]. For the various temperature tests, controlled temperature chambers having both heating and cooling capabilities were used. Temperature control was specified to be ±3 °C.

2.2. Electrical performance ratings of the ATD program Gen 1 lithium-ion cells

The ATD Gen 1 cell limits are the following.

Nominal rated cell capacity	0.9 Ah at a C_1/1 discharge rate
Discharge	
Minimum discharge voltage	3.0 V
Maximum discharge current	2.0 A continuous; 7.2 A (8 C) for up to an 18 s pulse; and 13.5 A (15 C) for up to a 2 s pulse
Maximum discharge temperature	70 °C
Charge and regen	
Maximum charge/regen voltage	4.1 V continuous; 4.3 V for up to a 2 s pulse
Maximum charge/regen current	0.9 A continuous charge current; 12 A maximum regen current for up to a 2 s pulse
Maximum charge temperature	40 °C
Maximum regen temperature	70 °C
Recharge procedure	Charge at 0.9 A (C_1/1) constant-current rate to a voltage of 4.1 V; continue to apply a constant-voltage of 4.1 V for 2.5 h total recharge time. All recharging is to begin at 25 ± 3 °C

2.3. Electrical performance tests

Characterization tests were performed on all the cells following a pre-test readiness review. The characterization tests included a C_1/1 static capacity test (some of the cells also underwent a C_1/25 discharge test); low- and medium-current hybrid power pulse characterization (L-HPPC and M-HPPC, respectively) tests for 18 s at discharge currents of 2.7 and 7.2 A, respectively; and a 7-day self-discharge test at 3.660 V, which corresponds to 50% SOC. Thermal performance tests consisting of the static capacity and L-HPPC tests were performed on four cells at ambient temperatures of +5 and +40 °C. Finally, reference performance tests (RPTs) were conducted on all cells prior too beginning the life testing. The RPTs consisted of a single C_1/1 constant-current discharge, one M-HPPC test and ac impedance measurements at 1 kHz at 100 and 0% SOC. Cells were then designated for either the calendar- or cycle-life at a given condition. The cycle- and calendar-life tests where then conducted for a 4-week period for cells tested at 40, 50 or 60 °C, and for a 2-week period for those cells tested at 70 °C. The RPTs were repeated every 4 weeks for the cells tested at 40, 50 and 60 °C, and every 2 weeks for the cells tested at 70 °C. End-of-testing (EOT) was reached when a cell was unable to perform the M-HPPC test at 60% DOD or falling below the 3.0 V minimum cell voltage.

This paper will deal with the calendar- and cycle-life testing of these cells using special tests developed by the ATD program [2]. The special calendar-life test is theoretically charge-neutral, so it will not perturb the SOC of the cell any more than absolutely necessary. The magnitude and duration of the discharge and regen tests are relatively modest, compared with the corresponding M-HPPC test profile, so they would have a minimal affect on the thermal condition of the cell under test. The magnitude and duration of the discharge pulse for this test, i.e. 3.6 A for 9 s was set to one-half the corresponding values used for the M-HPPC test. The test incorporated a somewhat longer-than-normal rest period after the discharge pulse to allow additional time for voltage recovery before the regen pulse. This is a new calendar-life test designed to obtain additional resistance data at regular intervals without unduly cycling the cells. The idea was to apply a single pulse profile once per day from which the discharge and regen resistances could be calculated. The calendar-life test profile is shown in Table 1.

Table 1
ATD program special calendar-life test pulse profile

Step time (s)	Cumulative time (s)	Current (A)	Charge (A s)	Cumulative charge (A s)
9	9	3.6	32.40	32.40
60	69	0.00	0.00	32.40
2	71	−3.6	−7.20	25.20
2	73	0.00	0.00	25.20
47	120	−0.54	25.38	0.18

Note that positive values for the current correspond to a constant-current discharge and negative values correspond to a constant-current charge, i.e. regen pulse.

Each cell tested using the calendar-life test was assigned a temperature (40, 50, 60 or 70 °C) and a target SOC (either 60 or 80% SOC in this study). For a new cell, the cell voltage was 3.742 V at 60% SOC and was 3.918 V at 80% SOC. The value of the voltage at a given SOC was determined from a calibration table provided by ANL that showed the voltage at a given SOC, as found by conducting C_1/25 discharge tests on a number of new test cells. The discharge and regen resistances were calculated using $R = \Delta V/\Delta I$, i.e. the change of the voltage of the cell at the beginning of the discharge (or charge) to the end of the discharge (or charge) divided by the change in the current during the discharge (or charge). For the calendar-life tests (Table 1), the discharge or regen currents were held constant, but the voltage did change during the course of the discharge or recharge. The test was conducted once per day for a 4-week period for the 40, 50 and 60 °C tests, and for a 2-week period for the 70 °C test.

The special ATD program cycle-life test profiles (conducted at 60% SOC) for the Δ3, Δ6 and Δ9% SOC tests are given in Tables 2–4, respectively. Positive values of the current correspond to a discharge current, while negative values correspond to a charge current, i.e. regen. These profiles are charge neutral, as shown. The test profiles were conducted once the cell had reached the test temperature

Table 2
ATD program special cycle-life Δ3% SOC pulse test profile

Step time (s)	Cumulative time (s)	Current (A)	Charge (A s)	Cumulative charge (A s)
14	14	7.20	100.80	100.80
10	24	0.00	0.00	100.80
2	26	−6.48	−12.96	87.84
2	28	0.00	0.00	87.84
32	60	2.745	−87.84	0.00
20	80			

Table 3
ATD program special cycle-life Δ6% SOC pulse test profile

Step time (s)	Cumulative time (s)	Current (A)	Charge (A s)	Cumulative charge (A s)
14	14	7.20	100.80	100.80
10	24	0.00	0.00	100.80
2	26	−6.48	−12.96	87.84
2	28	0.00	0.00	87.84
14	42	7.2	100.80	188.64
10	52	0.00	0.00	188.64
2	54	−6.48	−12.96	175.68
2	56	0.00	0.00	175.68
64	120	2.745	−175.68	0.00
40	160			

Table 4
ATD program special cycle-life Δ9% SOC pulse test profile

Step time (s)	Cumulative time (s)	Current (A)	Charge (A s)	Cumulative charge (A s)
14	14	7.20	100.80	100.80
10	24	0.00	0.00	100.80
2	26	−6.48	−12.96	87.84
2	28	0.00	0.00	87.84
14	42	7.20	100.80	188.64
10	52	0.00	0.00	188.64
2	54	−6.48	−12.96	175.68
2	56	0.00	0.00	175.68
14	70	7.20	100.80	276.48
10	80	0.00	0.00	276.48
2	82	−6.48	−12.96	263.52
2	84	0.00	0.00	263.52
96	180	2.745	−263.52	0.00
60	240			

(either 40, 50, 60 or 70 °C). Each cell undergoing cycle-life testing was initially tested at the target temperature and 60% SOC for 100 iterations followed by a 1 h rest to verify stable SOC cycling. If the SOC cycling was stable, then the cycle-life test was resumed on a continuous basis for the remaining test period. Designated cells underwent the cycle-life testing for a 4-week period for the cells tested at 40, 50 and 60 °C, and for a 2-week interval for different cells tested at 70 °C. *C*/1 and M-HPPC reference tests (at 25 °C) were performed before and after the 4- or 2-week test interval.

3. Results and discussion

3.1. Calendar-life tests at 80% SOC

3.1.1. Discharge resistance

For the calendar-life tests conducted at 80% SOC (open-circuit voltage set at 3.918 V), cells were tested at both the INEEL and SNL. The data discussed here combined all of the available discharge and regen resistances as a function of test time as measured by each of the two laboratories. Note, however, that some of the cells tested under a given temperature condition failed prior to, or during, the calendar-life test. When this occurred, the data for that cell was not included in the averaged data presented below. The notation convention used in this paper to identify the test condition is (*xx*C*yy*), where *xx* gives the percentage SOC (either 60 or 80%) of the cell during the test, C signifies that it is a calendar-life test and *yy* specifies the test temperature (either 40, 50, 60 or 70 °C). Thus, (80C40) specifies a cell tested at 80% SOC, using the calendar-life test and tested at 40 °C. Fig. 1 shows the average of the INEEL and SNL (up to six cells) discharge resistances at 40, 50, 60 and 70 °C as a function of the square-root of the time at test temperature in days. The data shown is from the first 4-week test period for the 40, 50 and 60 °C tests, and for the first 2-week test period for the 70 °C test. In order to formulate a model of the behavior of the resistance data, a number of different time dependencies of the discharge and regen resistances were tried, but the square-root of test time was found to correlate the data the best. The functional forms examined were:

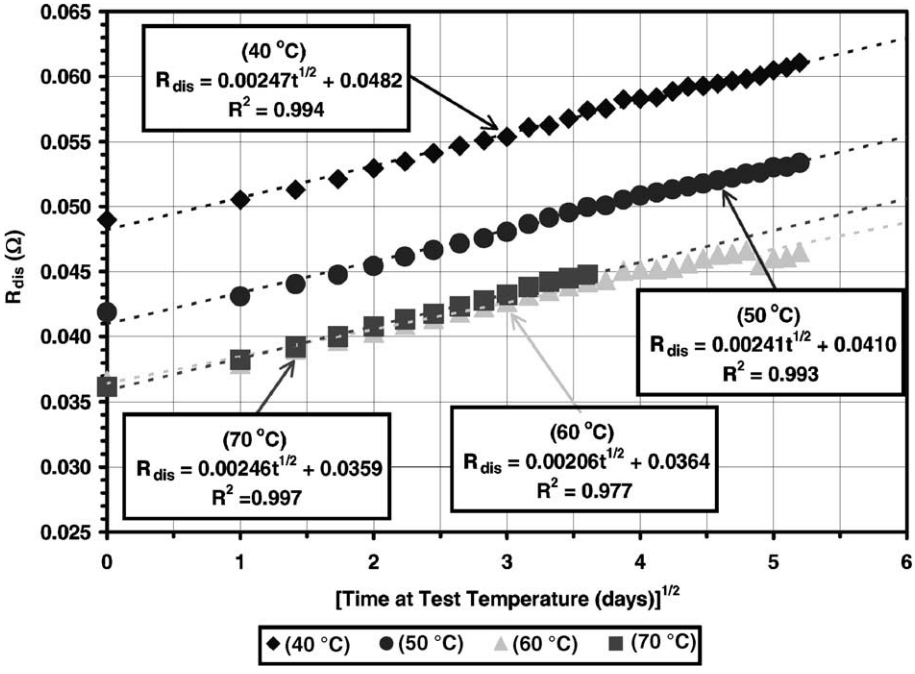

Fig. 1. Average of all INEEL and SNL data from calendar-life discharge resistance tests at (80C40, 80C50, 80C60 and 80C70) for ATD Gen 1 cells plotted as a function of the square-root of test time. The model fits to the relation: $R(t,T) = A(T)t^{1/2} + B(T)$ and the correlation coefficient (R^2) are given in the figure for each test temperature.

$R = At + B$; $R = At^2 + Bt + C$; $R = A[\exp(Bt)]$; $R = A[\ln(Bt)] + C$; $R = At^{3/2} + B$; $R = A[t^n]$, where n is a fitting parameter for the test time raised to a power. Higher order polynomial fits to the data would, of course, give better fits to the data, but the physical significance would be very hard to explain in terms of a physical/chemical model of the process(es) (refer to [5] for further details). Also shown in the Fig. 1 are the linear regression fits to the function $R_{dis} = At^{1/2} + B$, where A and B are the fitting parameters. The goodness-of-fit parameter is given by the value R^2, which is often referred too as the correlation coefficient. $R^2 = 1$ would be the best correlation of the data to the fitting function. In general, the discharge resistances decrease as the test temperature is increased. This is true for all of the data, except at 70 °C, where the resistance is slightly greater than that measured at 60 °C. One would expect that the resistance at this temperature would follow the general trend and be lower than at the other temperatures. The unusual 70 °C data behavior probably indicates that an additional mechanism (or mechanisms) responsible for cell degradation is (are) occurring at this temperature.

A functional form for the description of the time, temperature and SOC dependence of the discharge and regen resistance was, therefore, assumed to be as follows:

$$R(t, T, \mathrm{SOC}) = A(T, \mathrm{SOC})F(t) + B(T, \mathrm{SOC}) \quad (1)$$

where t is the time at test temperature (in days), T the test temperature and SOC the SOC of the battery at the start of the calendar-life test. $A(T, \mathrm{SOC})$ and $B(T, \mathrm{SOC})$ are assumed to be functions of the temperature and the SOC only. The function $F(t)$ is assumed to be only a function of the time at test temperature; the best fit of the resistance data being $F(t) = t^{1/2}$. The following results will concern the verification of this relationship and to find the functional forms for $A(T, \mathrm{SOC})$ and $B(T, \mathrm{SOC})$. Once these functions have been determined, then a physical/chemical basis for the functional forms is attempted using the fits to the discharge and regen resistances as a guide. The reason for plotting the data as various functions of test time was to try and determine not only the time dependence of the resistance increase, but also if the a functional form for the time dependence can be found, to ascertain a physical/chemical process that would account for the discharge and regen resistance increase with time. This information could then be used to understand the process(es) responsible for the cell degradation and in turn suggest possible changes in the construction of the cells. An additional aspect of the determination of the functional form of the time-dependent degradation would be to predict the calendar- and cycle-life of the cells at various test temperatures.

What are some of the mechanisms responsible for the resistance and increase in the resistance of a lithium-ion battery? Zhang et al. [8] and Wang et al. [9] have discussed the possible mechanisms. The total resistance of the carbon anode and the metal oxide cathode is the sum of the following resistances: (a) electrolyte solution; (b) surface layer; (c) anode and cathode particle to particle contact; (d) anode and cathode particle contact to the current collector; and (e) charge transfer. The interfacial impedance at the discharged state has been found to be larger when compared with the charged state for both the carbon and metal oxide electrodes. Experimental results using electrochemical impedance spectroscopy (EIS) show that the impedance of lithium-ion cells, at least with $LiCoO_2$ cathodes, is dominated by the positive electrode, i.e. the cathode. The total cell impedance was found to increases with a decrease in the SOC. Upon consideration of the multitude of possible mechanisms that can lead to resistance increases as the cell ages, the fact that a thin film, often referred too as the solid electrolyte interface (SEI) layer arising from the decomposition of the electrolyte and salt is a likely candidate. When the electrodes are in the charged state, there will be a large portion of Ni^{4+} and Co^{4+} cations present in the cathode. These ions have a strong oxidizing power and can react with the electrolyte and salt at the cathode/electrolyte interface. This reaction can cause decomposition of the electrolyte and salt to form a SEI layer on the cathode. After extended cycling, the $LiNi_{1-x}Co_xO_2$ electrode used in the ATD program Gen 1 cells should be heavily passivated, resulting in a large resistance at the electrolyte/cathode interface. Due to this increase in resistance, the reaction rate will be lower for both lithium-ion insertion (intercalation) and removal (de-intercalation).

The earliest reference to the SEI layer that the authors are aware of is that by Thomas et al. [10], who state that the polymeric surface layer, i.e. the SEI layer must be in a dynamic state that depends on cell temperature, SOC and the extent of aging of the cell. The resistances directly relate to the thickness of the surface layer. The SEI layer that forms on carbonaceous electrode materials consists of many different materials, including LiF, Li_2CO_3, LiCO–R, Li_2O, lithium alkoxides (Li–O–R, where R is a hydrocarbon), non-conductive polymers and a number of other possible chemical compounds composed of electrolyte and salt decomposition products. The formation of the SEI layer mainly occurs on the anode during the initial formation (charging) cycle of the battery. The implication of the SEI layer on the carbon electrode is that it will cause a voltage drop across the layer. This will in turn modify the structure of the double layer at the carbon electrode/electrolyte interface, which generally increases the charge transfer resistance at this interface. A SEI layer also forms on the cathode material that also results in an increase in the charge transfer at the electrolyte/cathode interface. Cycling will also cause capacity loss due to damage and disorder in the metal oxide cathode particles. Cycling can also induce severe strain, high defect densities and occasional fracture of the particles [8]. Severely strained cathode particles exhibit cation disorder. These processes lead to changes in the thermodynamic properties and contact resistance of the metal oxide particles. The accumulation of strain in the electrode particles may cause partial shedding of the electrode material from its

current collector. A portion of the lithium-ions in the cathode can also become inactive due to cation disorder. However, the main loss in the cathode, for example, $LiCoO_2$ is caused by the change in resistance at the surface of the particles.

Arora et al. [11] have also discussed some of the processes known to result in capacity fade in lithium-ion cells. These are lithium deposition on the anode (over-charge condition), electrolyte decomposition, anode and/or cathode active material dissolution, phase changes in the anode and cathode materials and passive film formation over the electrode and current collector surfaces (SEI layer formation). They found that the ionic conductivity of the electrolyte does not contribute significantly to the cell's overall conductivity. This was substantiated by the work of Narayanan et al. [12] who state that the process of lithium-ion diffusion in the anode and cathode lattice is considerably slower that that in the electrolyte. Therefore, the lithium-ion diffusion in the electrode materials would be one of the rate-limiting steps. Thus, the processes affecting the cell impedance directly relate to the electrode materials and their interactions with the electrolyte, i.e. the SEI layer. Ozawa [13] and Megahed and Scrosati [14] have also discussed and confirmed these processes. Nagasubramanian et al. [15] and Baker et al. [16], using EIS methods find that the impedance increase with aging is mostly due to the cathode. They also found that the interfacial impedance increases as the SOC of the cell decreases. From their measurements, they find that the cell impedance comes mostly from the cathode/electrolyte interface, not from the anode/electrolyte interface. Guyomard and Tarascon [17] conclude that oxidation of the electrolyte is the main failure mechanism for lithium-ion batteries.

The extensive work of Auerbach and co-workers [18,19] has also given an overview of the processes occurring in a lithium-ion cell. They state that in parallel to the flux of lithium-ions to and into the electrodes, there is a flux of electrons from the current collector to the anode or cathode materials, which balances the charge. This electron flux also has to overcome the resistance that exists among the electrode particles, all of which are partially covered by electronically insulating surface films, i.e. a SEI layer. Lithium intercalation into the graphite anode or the metal oxide cathode is a serial multi-step process in which lithium-ions have to first migrate through the electrolyte and then through the surface films that covers the electrodes. After this migration, insertion into the electrode material is accompanied by a charge transfer at the film/electrode material interface. This is then followed by solid state diffusion of lithium into the bulk of the electrode material. Finally, lithium accumulates within crystallographic sites in the bulk electrode material via phase transition(s) between the various intercalation stages. The intercalation stages, particularly for the metal oxide, depend on the crystalline structure of the electrode material. The process of charge transfer resistance can be related to three different processes: (1) Li-ion transfer at the solution-surface film interface; (2) Li-ion transfer at the surface film/electrode interface; and (3) inter-particle electron transfer between the particles constituting the electrode material. They also state that the increased resistance observed upon cycling the battery mostly reflects changes in the surface structure of the electrodes. After prolonged cycling, there are phenomena such as expansion and contraction of the electrode material's volume, which leads to local breakdown of the passivation layer of the electrode (on a microscopic level). This allows continuous reduction and oxidation of the electrolyte/solute species. While the process occurs on a very small scale, it thickens the surface films and consequently the electrode's impedance increases, particularly in the time constants that relate to lithium-ion migration through the surface films, whose increasing thickness upon cycling makes them more resistive. The electrolyte composition has a great impact on the surface films and, depending on its composition, the surface films may be the dominant factor that determines the impedance of the electrodes. However, this behavior may not be stable, i.e. the electrode's impedance, especially in the features that relate to the surface films, increases upon storage, and may also change as a result of thermal cycling and the charging and discharging of the battery.

In summary, the overall insertion process of lithium into the battery electrodes is quite complicated. It includes diffusion of lithium-ions in the solution phase, their migration through the surface films (SEI layer) covering the electrode particles (which are ionically conducting but electrically insulating to electron flow), solid state diffusion, accumulation/consumption of lithium in the bulk (accompanied by a flux of electrons that counterbalance the charge), and finally phase transition(s) among the crystalline structures of the electrode materials. Thus, a lithium-ion battery is a very dynamic system whose electrical performance depends on its construction, the materials used in its assembly, the rates of charge and discharge during use, the SOC, and its temperature. One physical/chemical process that stands out as a candidate for having the greatest impact on the impedance of the cell is the SEI layer, its growth, composition, structure and thickness. These attributes will also change as the cell ages.

Looking at possible analogous processes that grow thin films upon a solid surface, one can consider the oxidation of metals [19–21]. Upon examination of the various reaction rates and corresponding rate equations for the oxidation of metals, it is found that they are functions of a number of factors, such as material composition, temperature, oxygen pressure, elapsed time of reaction, surface preparation and pre-treatment of the metal. Although rate equations alone are insufficient for interpretations of oxidation mechanisms, these equations may be used to classify the oxidation of metals and may as such often limit the interpretation to a class of alternative mechanisms. The rate equations most commonly encountered may be classified as logarithmic, parabolic and linear. They represent only limiting and ideal cases. Deviations from these rate equations and intermediate rate equations are also often encountered. In many instances,

it may be difficult to fit rate data to any simple rate equation or combination of rate equations. In the following discussion, an analogy is made between a process occurring at the various surfaces present in a lithium-ion battery, the exact nature having been, as yet, not definitively determined and the growth of an oxide film on a metal surface [19–22]. Of the various oxidation processes that have been observed, the parabolic rate process has been identified and has the functional form:

$$X \propto t^{1/2} \tag{2}$$

where the thickness of the thin film (X) is proportional to the square-root of the time that the film growth has occurred. Blomgren [23] has used this argument to account for the capacity fade of the lithium-ion batteries that he has studied. As a rule, parabolic oxidation signifies that a thermal diffusion process is rate determining [19,20]. Thermal diffusion processes generally have a temperature dependence given by an Arrhenius-like process where the diffusion is given by [24–27]:

$$D = D_0\left[\exp\left(-\frac{E}{RT}\right)\right] \tag{3}$$

where D is the diffusion constant in cm^2/s, D_0 the limiting diffusion constant at very high temperature, E the activation energy associated with the diffusion process, R the gas constant and T the temperature (K). Such a process may include a uniform diffusion of one or both of the reactants through a growing scale or a uniform diffusion of gas into the metal.

The analogy to the case of the lithium-ion battery is that there would be a film growing on the surface of the anode and/or cathode materials over a period of time that would be temperature- and possibly SOC-dependent. The nature of the thin film would also depend on the electrolyte and the composition of the electrodes. The thickness of this thin film could give rise to an increase in the resistance of the cell as the rate of lithium migration into/out of the anode and/or cathode materials would be impeded by the thin film. The thicker the thin film, the lower the mobility of the lithium-ions and thus the higher the resistance.

The best fit to the time dependence of the resistance, as previously discussed, is the square-root of the time at test temperature as shown in Fig. 1. It may well be that as the cell ages the SEI layer grows in thickness, leading to an increase in the resistance, due to a decrease in the migration rate of the lithium-ions into/out of the anode and/or the cathode. The stresses experienced by the cathode particles during change and discharge, and during temperature variation, could lead to fracturing of the particles, as mentioned. This would effectively expose new surfaces on which a SEI layer would grow, thus increasing the anode and/or cathode resistance. This resistance would be observed as an increase of the discharge and charge resistances measured during the calendar-life test. If the increase in the discharge and regen resistance is proportional to the square-root of time at test temperature, then the resistances can be expressed by a function having the form (from Eq. (1)):

$$R(t, T, \mathrm{SOC}) = A(T, \mathrm{SOC})t^{1/2} + B(T, \mathrm{SOC}) \tag{4}$$

where the discharge and regen resistance ($R(t, T, \mathrm{SOC})$) is a function of time (t), test temperature (T) and SOC. That there is a dependence on the SOC is verified by comparing the discharge and regen resistance when the calendar-life test is conducted at 80 or 60% SOC (discussed later in this paper). The functions $A(T, \mathrm{SOC})$ and $B(T, \mathrm{SOC})$ are assumed to be functions of the test temperature and SOC. To determine the temperature dependence of the functions $A(T, \mathrm{SOC})$ and $B(T, \mathrm{SOC})$, one can plot the fitting coefficients determined from the fits shown in, for example, Fig. 1 as various function of the test temperature. Shown in Fig. 2 is a plot of the function $A(T, \mathrm{SOC})$ for the discharge resistance determined from the fits shown in Fig. 1 as a function of the inverse of the test temperature (K). Other functional dependencies were examined [5], but this relation fit the $A(T, \mathrm{SOC})$ parameter the best. In Fig. 2, the $A(T, \mathrm{SOC})$ parameter is plotted as an inverse function of the temperature (K) using an exponential fit, i.e. $A(T, \mathrm{SOC}) = a(\mathrm{SOC})\{\exp[b(\mathrm{SOC})/T]\}$ where the fitting parameters a and b are shown as being function of the SOC of the battery. This type of function occurs in a number of physical/chemical processes, such as chemical kinetics and in diffusion. A functional form of this kind is generally referred too as Arrhenius-like behavior, as it applies to a chemical reaction or to a diffusion-type of process. The fit of $A(T, \mathrm{SOC})$ to this functional form of the temperature is quite good for 40, 50 and 60 °C, but the 70 °C value does not fall on the fitting curve. The fits to the exponential function given in Fig. 2 are given for when only the 40, 50 and 60 °C data are used, and also for when all the temperature data are used, i.e. the 40, 50, 60 and 70 °C data. The values of the fitting parameters and the R^2 value are given in the figure. Using, then, the fit to the exponential of the inverse temperature, the A parameter can be expressed as:

$$A(T, \mathrm{SOC}) = a(\mathrm{SOC})\left\{\exp\left[\frac{b(\mathrm{SOC})}{T}\right]\right\} \tag{5}$$

where $a(\mathrm{SOC})$ is the fitting coefficient having the units of $(\Omega/t^{1/2})$ and $b(\mathrm{SOC})$ has the units of temperature (K). The b fitting parameter can be related to an activation energy ($E_{\mathrm{dis},A}$) using $b = E_{\mathrm{dis},A}/R$ where R is the gas constant equal to 8.314 J/(mol K) (or 1.987 cal/(mol K)).

Similarly, the discharge $B(T, \mathrm{SOC})$ parameters from the fits to the data shown in Fig. 1 are plotted as a function of the inverse of the test temperature (K) (Fig. 3). Two fits are again shown, one for when only the 40, 50 and 60 °C data are used and one for when all of the temperatures are used. Again, the 70 °C value does not correlate well with the other temperatures. The most reasonable fit to the discharge $B(T, \mathrm{SOC})$ parameter was thus found to be given by the expression:

$$B(T, \mathrm{SOC}) = c(\mathrm{SOC})\left\{\exp\left[\frac{d(\mathrm{SOC})}{T}\right]\right\} \tag{6}$$

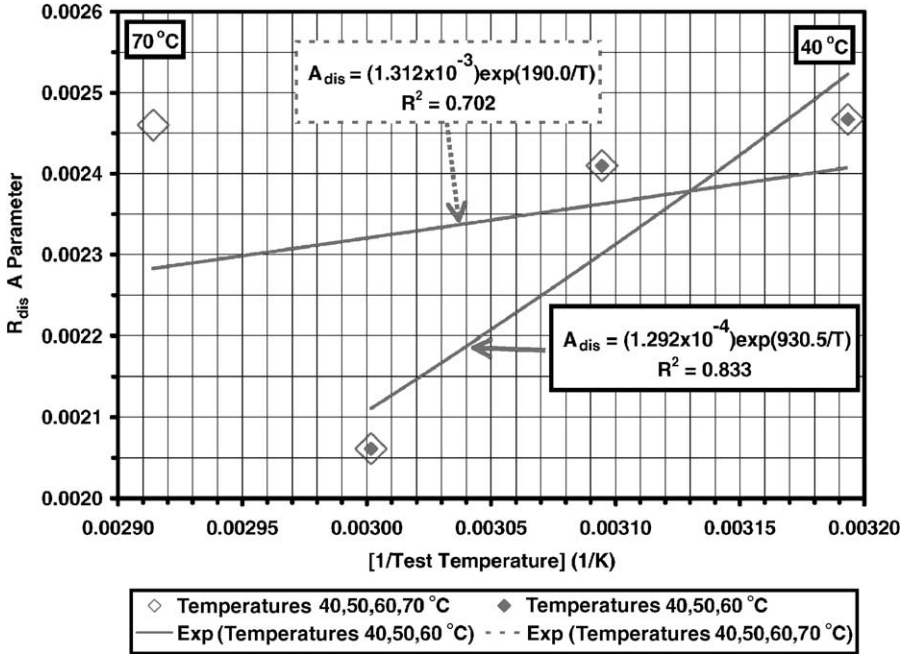

Fig. 2. $A(T)$ parameter for the tests (80C40, 80C50, 80C60 and 80C70) from data fits to the model $R(t,T) = A(T)t^{1/2} + B(T)$ is shown as a function of the inverse test temperature (K). Fitting parameters to the model $A(T) = a[\exp(b/T)]$ are given. The fits to when all the test temperatures are used and when only the 40, 50 and 60 °C data are used are shown.

where c(SOC) is a coefficient having the units in Ω and d(SOC) is the fitting parameter having the units of temperature (K). As before, the c and d parameters are shown to possibly be functions of the SOC of the battery. The b parameter can be related to an activation energy using $b = E_{\mathrm{dis},B}/R$, where R is again the gas constant. Other functions for the temperature dependence of $A(T, \mathrm{SOC})$ and $B(T, \mathrm{SOC})$ were examined, but the exponential of the inverse of the test temperature was found to be the best [5].

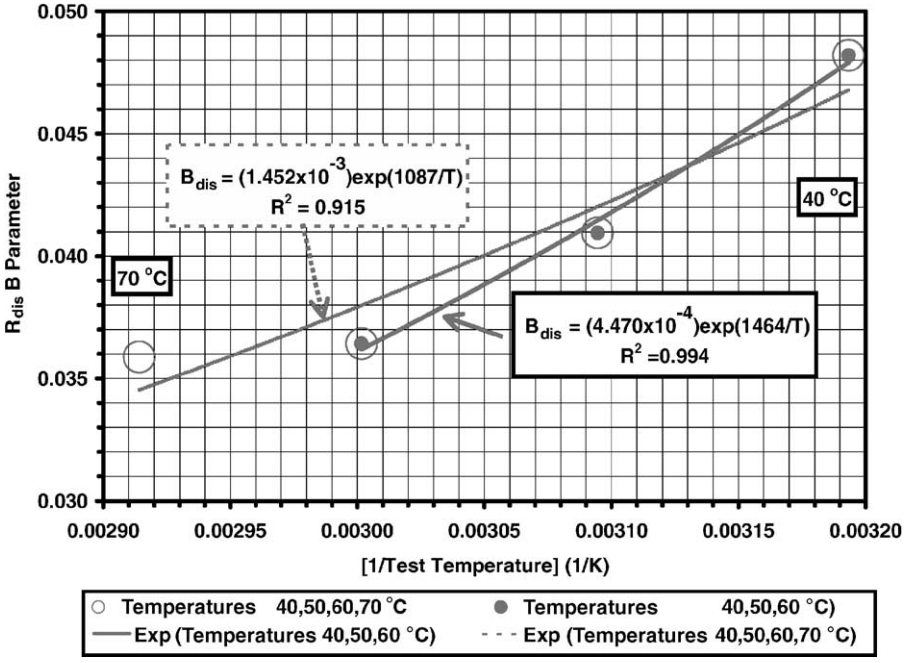

Fig. 3. $B(T)$ parameter for the tests (80C40, 80C50, 80C60 and 80C70) from data fits to the model: $R(t,T) = A(T)t^{1/2} + B(T)$ is shown as a function of the inverse test temperature (K). Fitting parameters to the model $B(T) = c[\exp(d/T)]$ are given. The fits to when all the test temperatures are used and when only the 40, 50 and 60 °C data are used are shown.

Table 5
Values of E_{act} at 80% SOC from analysis of calendar-life test data using the relationship: $R(t, T) = A(T)t^{1/2} + B(T)$, where $A(T) = a[\exp(E_{act,A}/RT)]$ and $B(T) = c[\exp(E_{act,B}/RT)]$

Test condition	Activation energy ($E_{act,A}$, kJ/mol)	Activation energy ($E_{act,B}$, kJ/mol)
R_{dis} (80C40, 80C50, 80C60 and 80C70)	1.58 (0.378)	9.04 (2.16)
R_{dis} (80C40, 80C50 and 80C60)	7.74 (1.85)	12.2 (2.91)
R_{reg} (80C40, 80C50, 80C60 and 80C70)	4.36 (1.04)	9.20 (2.20)
R_{reg} (80C40, 80C50 and 80C60)	8.03 (1.92)	12.9 (3.08)

E_{act} are activation energies, and a and c are pre-exponential constants. The values given in parenthesis are in kcal/mol.

Table 6
Values of the pre-exponential constants a and c at 80% SOC from analysis of calendar-life test data analysis using the relationship: $R(t, T) = A(T)t^{1/2} + B(T)$, where $A(T) = a[\exp(E_{act,A}/RT)]$ and $B(T) = c[\exp(E_{act,B}/RT)]$

Test condition	Pre-exponential constant a ($\times 10^{-4}\ \Omega$ per (day)$^{1/2}$)	Pre-exponential constant c ($\times 10^{-4}\ \Omega$)
R_{dis} (80C40, 80C50 and 80C60)	1.29	4.47
R_{reg} (80C40, 80C50 and 80C60)	1.03	2.68

The values for the activation energies and the pre-exponential constants determined from the fits to $A(T, \text{SOC})$ and $B(T, \text{SOC})$ for both the discharge and regen resistance are given in Tables 5 and 6. Note that the parameters a, b, c and d can be SOC-dependent, which is indeed the case, as will be shown when the calendar-life 60% SOC discharge and regen resistance data are analyzed. However, it should be restated that since the calendar-life tests were only conducted at two SOC, a model for the SOC dependence could not be determined, as only two data points were available. The final relationship for the discharge (and regen) resistance is, therefore, the following:

$$R(t, T, \text{SOC}) = a(\text{SOC})\left\{\exp\left[\frac{b(\text{SOC})}{T}\right]\right\}t^{1/2} + c(\text{SOC})\left\{\exp\left[\frac{d(\text{SOC})}{T}\right]\right\} \quad (7)$$

Fig. 4 shows the model's predictions using Eq. (7) for the case when all of the temperature values (40, 50, 60 and 70 °C) are used in determining a, b, c and d for the discharge resistance. The raw data values are the same as shown in Fig. 1 and are

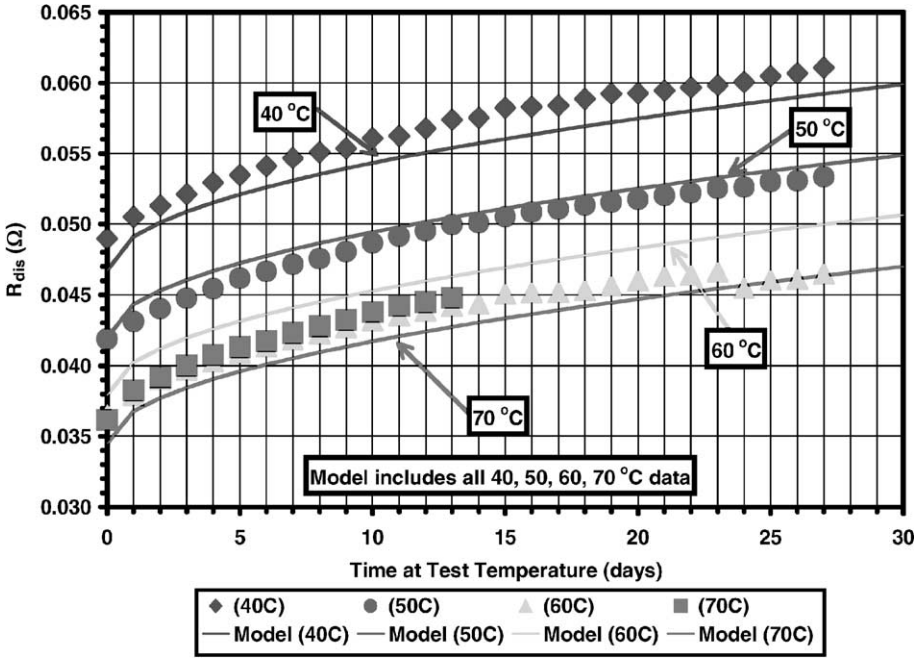

Fig. 4. Model predictions compared to calendar-life discharge resistance data for ATD Gen 1 (80C40, 80C50, 80C60 and 80C70) tests with the a, b, c and d parameters determined when all the test temperatures were used to fit the resistance data.

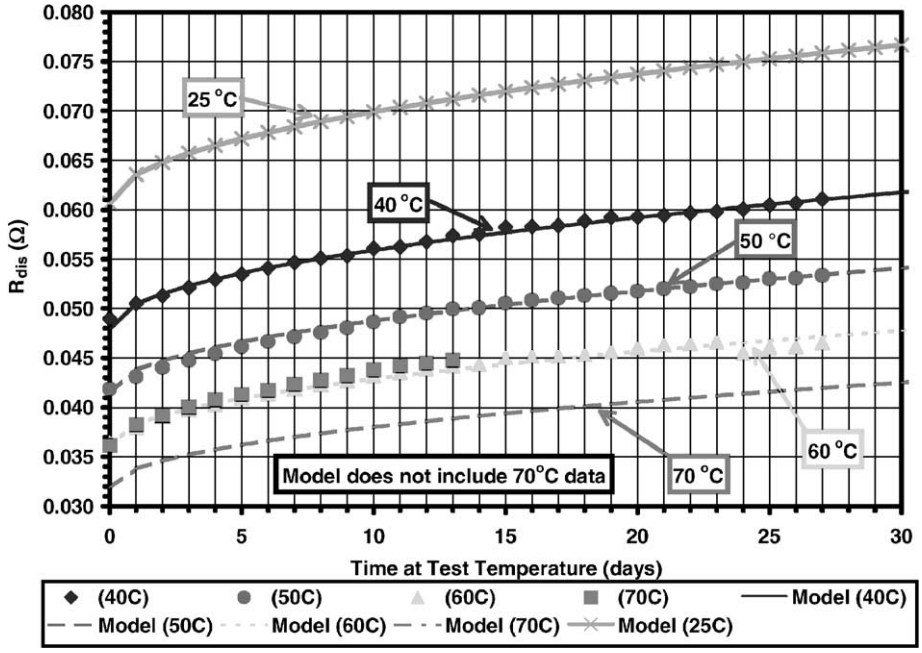

Fig. 5. Model predictions compared to calendar-life discharge resistance data for ATD Gen 1 (80C40, 80C50, 80C60 and 80C70) tests with the *a*, *b*, *c* and *d* parameters determined when only the 40, 50 and 60 °C test temperatures were used to fit the resistance data. The model prediction for a test temperature of 25 °C is also shown.

presented with the model predictions. The fits are not bad, but the 70 °C data are not well correlated, as should be the case, as previously discussed. Fig. 5 shows fits to the discharge resistance data using the model given in Eq. (7) when the values for *a*, *b*, *c* and *d* were determined using only the 40, 50 and 60 °C resistance data. This model gives excellent fits to the 40, 50 and 60 °C resistance data. The model using these fitting parameters does not fit the 70 °C, as would be expected. Also included in this figure are the model predictions for the discharge resistance as a function of time at test temperature when the test temperature is 25 °C.

3.1.2. Regen resistance

This section treats the regen resistance for the calendar-life testing at 80% SOC of the ATD Gen 1 cells. The same approach was used as was used for the treatment of the discharge resistance at 80% SOC. All of the regen resistance data for the four test temperatures for all the INEEL and SNL tested cells is given in Reference [5] and will not be reproduced here. Fig. 6 shows the average of all of the available regen resistance data at each of the four test temperatures for the first 4-week period at 40, 50 and 60 °C, and for the first 2-week period at 70 °C. As was the case for the discharge resistance, the regen resistance increased non-linearly with increasing time at test temperature. The regen resistance was smaller the higher the test temperature, as was also the case with the discharge resistance. The regen resistance was also smaller than the discharge resistance at each of the respective test temperatures. The 70 °C resistance, as shown in Fig. 6, did not follow the general trend of the other temperatures in that the resistance was the same or higher than the 60 °C temperature resistance. This trend for the 70 °C regen data is the same as was observed for the 70 °C discharge resistance (Fig. 5). This indicates again that something has happened to the cells at this test temperature compared to the lower test temperatures. The detailed nature of the process(es) responsible for this increase in the resistance is (are) not presently known.

The same approach was used to analyze the regen resistance at the various temperatures. The relations as given in Eqs. (1)–(6) were also found to best correlate the time and temperature dependence of the regen resistance, but with different values of the fitting parameters *a*, *b*, *c* and *d*. The best correlation to the time dependence of the regen resistance was obtained using a square-root of the time at test temperature, as was found to be the case for the discharge resistance. The fits to this time dependence, the fitting parameters, and the goodness-of-fit values are also shown in Fig. 6. The fits are quite good for all of the test temperatures. Thus, for the regen resistance, the functional form for the time dependence is that given by Eq. (4), which was also used for the discharge resistance. The fitting parameters for each temperature, i.e. the slope being $A(T, \text{SOC})$ and the intercept being $B(T, \text{SOC})$, were then used to determine the temperature dependence of *A* and *B* as before. As was the case for the discharge resistance, the most meaningful temperature dependence for $A(T, \text{SOC})$ and $B(T, \text{SOC})$ was to use an Arrhenius-like function to determine the temperature dependence of $A(T, \text{SOC})$ and $B(T, \text{SOC})$, as given by Eqs. (5) and (6). The values for the fitting coefficients are given in Tables 5 and 6. The best overall correlation to the regen resistance was when fits to the 70 °C data

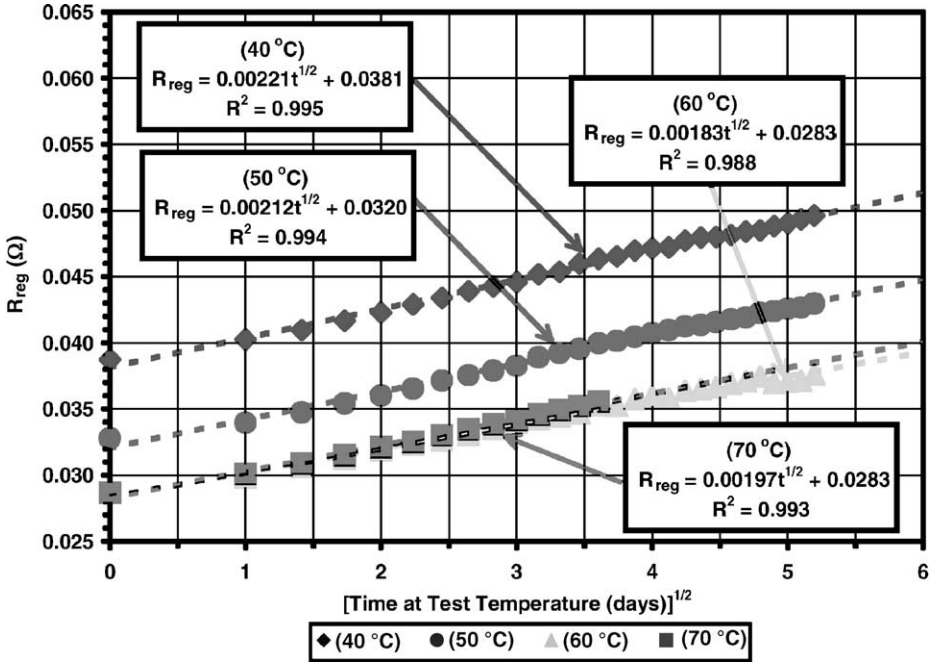

Fig. 6. Average of all INEEL and SNL data from calendar-life regen resistance tests at (80C40, 80C50, 80C60 and 80C70) for ATD Gen 1 cells plotted as a function of the square-root of test time. The model fits to the relation: $R(t, T) = A(T)t^{1/2} + B(T)$ and the correlation coefficient (R^2) are given in the figure for each temperature.

were excluded from the model. Fig. 7 shown the predictions of the model using Eq. (7) and the parameter values given in Tables 5 and 6 for when only the 40, 50 and 60 °C data fits are used. Also shown in Fig. 7, is the prediction of the model when the test temperature is 25 °C. The model predictions shown in Fig. 7 for the regen resistance can be compared to the model predictions shown in Fig. 5 for the discharge resistance. Overall, the discharge resistance is greater than the regen resistance at all times at test temperature and at all test temperatures.

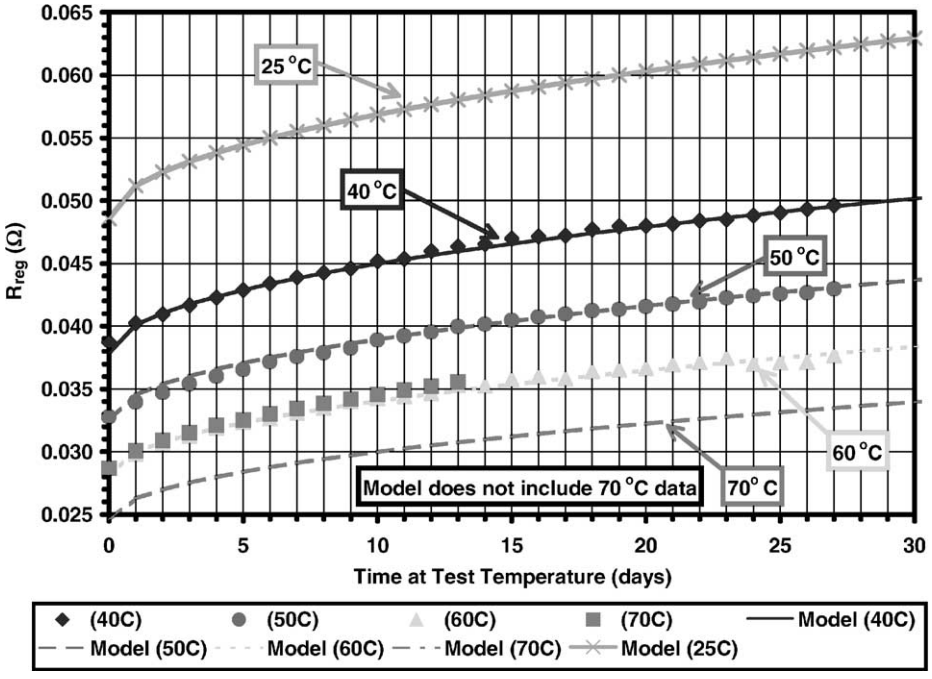

Fig. 7. Model predictions compared to calendar-life regen resistance data for ATD Gen 1 (80C40, 80C50, 80C60 and 80C70) tests. Model predictions are shown with the *a*, *b*, *c* and *d* parameters determined when only the 40, 50 and 60 °C test temperatures were used to fit the resistance data. The model prediction for a test temperature of 25 °C is also shown.

Table 5 shows the activation energies for both the discharge and regen resistance data as determined using Eq. (7) with the square-root of test time at temperature time dependence and the exponential of the inverse temperature for the temperature dependence. Given in this table are the activation energies for $A(T, \text{SOC})$ and $B(T, \text{SOC})$ for when the 70 °C data were used in the data fits and for when only the 40, 50 and 60 °C data were used to determine the parameters. The fits to the 40, 50 and 60 °C data are the best ones to consider based on the observations discussed. Upon examination of the activation energies given in Table 5, general trends for the activation energies are that the discharge and regen values are approximately the same order of magnitude for $E_{\text{act},A}$ and for $E_{\text{act},B}$. The activation energies for $E_{\text{act},B}$ are larger than for $E_{\text{act},A}$. The activation energies for R_{dis} and R_{reg} are approximately the same within experimental error for both $E_{\text{act},A}$ and $E_{\text{act},B}$. There is presently no explanation for the order of magnitude of these values or why the $E_{\text{act},B}$ values are greater than the $E_{\text{act},A}$ values. Fellner et al. [28] have discussed measurements on a battery when the cathode was a mixture of $LiNiO_2$ and $LiCoO_2$, the electrolyte was a mixture of PC, EC and DMC with $LiPF_6$, and the anode was a mixture of two different carbons. They observed that the interfacial resistance for a cell was much higher at lower temperatures and that the interfacial resistance appeared to grow linearly with test cycle number. The interfacial resistance had an activation energy of 63.5 kJ/mol. This value for the activation energy was attributed to an activated rate process such as solid state diffusion and/or electrochemical kinetics. The present authors have been unable to find literature values for lithium-ion diffusion through the SEI layer on the anode or cathode, or its diffusion in the anode or cathode materials for the compositions used in the ATD Gen 1 cells.

For completeness, the values of the pre-exponential constants obtained from the fits for the case of only using the 40, 50 and 60 °C data in the fits are shown in Table 6. The values for the pre-exponential parameters a and c are greater for the discharge resistance than for the regen resistance. At present, there is no explanation for these values based on a physical/chemical model, nor have literature values been found that may provide insight into the values.

3.2. Calendar-life tests at 60% SOC

This section discusses the discharge and regen resistance acquired when the cells were at 60% SOC. The test pulse sequence was that shown in Fig. 1. The tests were conducted at four temperatures: 40, 50, 60 and 70 °C, using the same testing protocols used for the 80% SOC tests discussed previously.

3.2.1. Discharge and regen resistance

This section discusses the calendar-life test (see Fig. 1 for the discharge/charge test sequence) when the cells were at 60% SOC (open-circuit voltage of 3.747 V for new cells). All of the test data were acquired at the INEEL. Initially, three cells were tested at each of the four temperatures: 40, 50, 60 and 70 °C. The same methodology was used to analyze these data as was used to analyze the 80% SOC discharge and regen resistance. Further details of the procedure and the results can be found in [5]. At this SOC, it was observed that there was an onset of a new process that affected the resistance values at 60 and 70 °C. The discharge and regen resistance data as a function of time at test temperature are shown in Figs. 8 and 9, respectively. The best fits to the data using the model given in Eq. (7) are also shown. Tables 7 and 8 present the fitting parameters determined from the model for the 60% SOC calendar-life tests. As can be observed for the discharge resistance, the model to the 40 and 70 °C are quite good. However, the discharge resistance at 60 °C was measured to be greater than the 50 °C resistance. The model, however, does bracket the data, but predicts that the 50 °C discharge resistance should be greater than the 60 °C discharge resistance. The 60 °C regen resistance data is smaller than the 50 °C resistance as would be expected, but still appears to be anomalous. It was also assumed that the 60 °C data does not follow the general trend of the other temperatures due to an unusual process occurring at this temperature. There was no great improvement [5] in the correlation of the model with the data when the 60 °C data was excluded as compared to when all the test temperatures are used to fit $A(T, \text{SOC})$ and $B(T, \text{SOC})$ in the model. This effect may well be a result of the SOC influence on the behavior of the cell. This influence may cause new processes to occur at different temperatures, depending on the SOC of the cell. As noted when discussing the 80% SOC data, it may also be the case that the 70 °C resistance data are also unusual due to the same or similar processes responsible for the behavior during testing at this SOC.

The values for the activation energies derived from the fits to the (60C40, 60C50, 60C60 and 60C70) test discharge and regen resistance data sets are shown in Table 7. These values compared to the (80C40, 80C50 and 80C60) test values (see Table 5) are of the same order of magnitude and are of comparable value. The $E_{\text{act},B}$ values are smaller at (60C40, 60C50, 60C60 and 60C70) than they are at (80C40, 80C50 and 80C60). This difference could partially account for the lower discharge and regen resistance at 60% SOC than at 80% SOC. The exponential of the activation energy divided by the temperature term, however, is only one part of the total resistance formula as given by Eq. (7). One also has to consider the pre-exponential factors. The pre-exponential factors as determined from the data for the (60C40, 60C50, 60C60 and 60C70) tests are given in Table 8.

3.3. Cycle-life discharge and regen resistance as a function of test time, Δ% SOC and test temperature

The cycle-life test at 60% SOC was only conducted at the INEEL. The following data combined all of the available discharge and regen resistances. Note, however, that some of

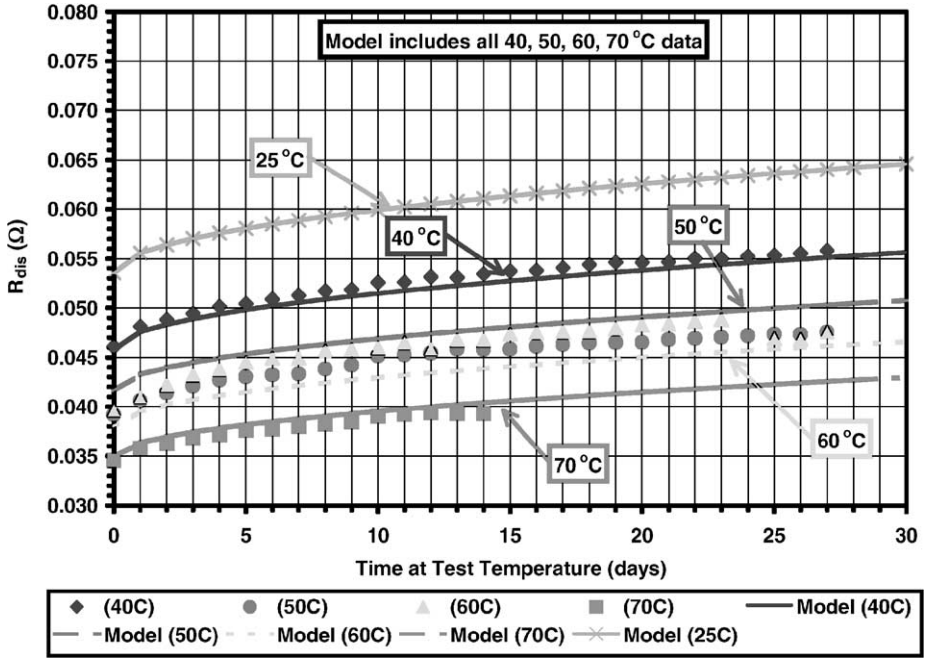

Fig. 8. Model predictions compared to calendar-life discharge resistance data for ATD Gen 1 (60C40, 60C50, 60C60 and 60C70) tests. Model used the *a*, *b*, *c* and *d* parameters determined when all the test temperatures were used to fit the resistance data. The model prediction for a test temperature of 25 °C is also shown.

the cells tested under a given temperature and Δ% SOC condition failed prior too, or during, the cycle-life test. When this occurred, the data for that cell was not included in the averaged data presented below. The notation convention used in this paper to identify a cycle-life test is the same as used for the calendar-life except that *Z* in (*xxZyy*) is replaced by 3, 6 or 9 and signifies that it is a cycle-life test at either Δ3, Δ6 or Δ9%. Thus, (60340) would specify a cell tested at 60% SOC, using the Δ3% SOC swing cycle-life test and tested at 40 °C.

Similar to the calendar-life modeling discussed previously, Fig. 10 shows the average discharge (designated R_{dis})

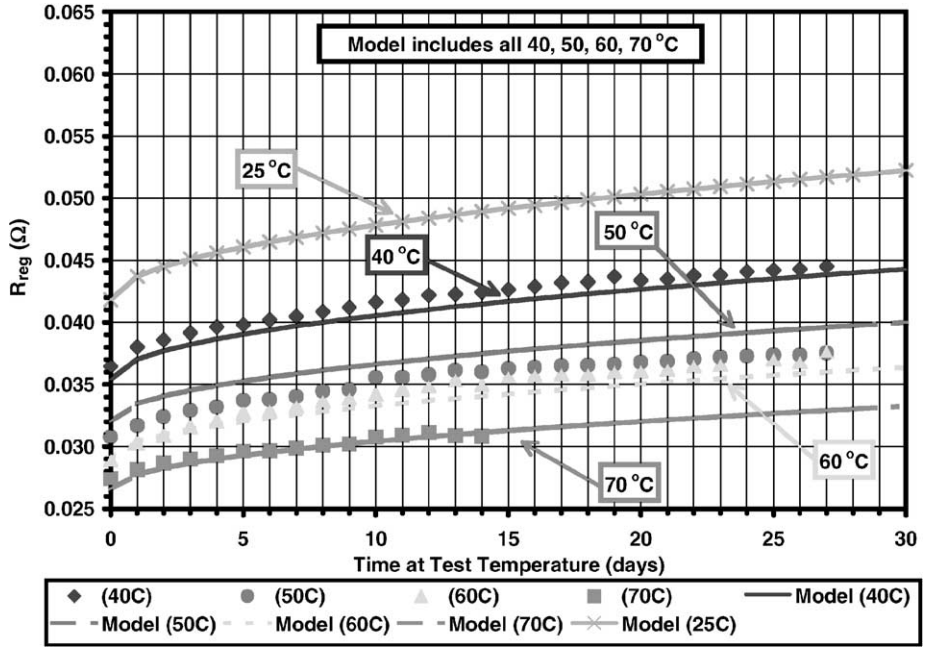

Fig. 9. Model predictions compared to calendar-life regen resistance data for ATD Gen 1 (60C40, 60C50, 60C60 and 60C70) tests. Model used the *a*, *b*, *c* and *d* parameters determined when all the test temperatures were used to fit the resistance data. The model prediction for a test temperature of 25 °C is also shown.

Table 7
Values of E_{act} at 60% SOC from analysis of calendar-life test data using the relationship: $R(t, T) = A(T)t^{1/2} + B(T)$, where $A(T) = a[\exp(E_{act,A}/RT)]$ and $B(T) = c[\exp(E_{act,B}/RT)]$

Test condition	Activation energy ($E_{act,A}$, kJ/mol)	Activation energy ($E_{act,B}$, kJ/mol)
R_{dis} (60C40, 60C50, 60C60 and 60C70)	5.88 (1.41)	8.11 (1.94)
R_{reg} (60C40, 60C50, 60C60 and 60C70)	8.35 (2.00)	8.59 (2.05)

E_{act} are activation energies, and a and c are pre-exponential constants. The values given in parenthesis are in kcal/mol.

Table 8
Values of the pre-exponential constants a and c at 60% SOC from analysis of calendar-life test data using the relationship: $R(t, T) = A(T)t^{1/2} + B(T)$, where $A(T) = a[\exp(E_{act,A}/RT)]$ and $B(T) = c[\exp(E_{act,B}/RT)]$

Test condition	Pre-exponential constant a (Ω per (day)$^{1/2}$)	Pre-exponential constant c ($\times 10^{-3}\ \Omega$)
R_{dis} (60C40, 60C50, 60C60 and 60C70)	1.88×10^{-4}	2.03
R_{reg} (60C40, 60C50, 60C60 and 60C70)	6.56×10^{-5}	1.31

and regen (designated R_{reg}) resistances as a function of the square-root of time at test temperature at 60% SOC, Δ3% SOC swing and at test temperatures of 40, 50, 60 and 70 °C. Note that each data point shown represents the discharge or regen value measured after 100 cycle-life cycles had been completed, i.e. between the data points shown, 100 test cycles were done. Note, as pointed out later, that it was assumed that all tests at a given temperature were actually done at that temperature. There was, however, some variation in the test temperatures for a given cell at a nominally specified target test temperature. This variation in the test temperature was not accounted for in Fig. 10, as the variation was usually only several °C. This temperature variation is, however, addressed in the detailed treatments of the data presented below. The averaged data shown in Fig. 10 have also been corrected for the time it took the cells to stabilize, which is why all data start at approximately time = 0 h. In general, the resistance decreases as the temperature is increased. This is true for all data except that at 70 °C, where the resistance is slightly greater than that measured at 60 °C. One would expect that the resistance at this temperature would follow the general trend and be lower than at the other temperatures. The unusual behavior of the 70 °C data probably indicates that an additional mechanism (or mechanisms) responsible for cell degradation is (are) occurring at this temperature. This was also found to be the case

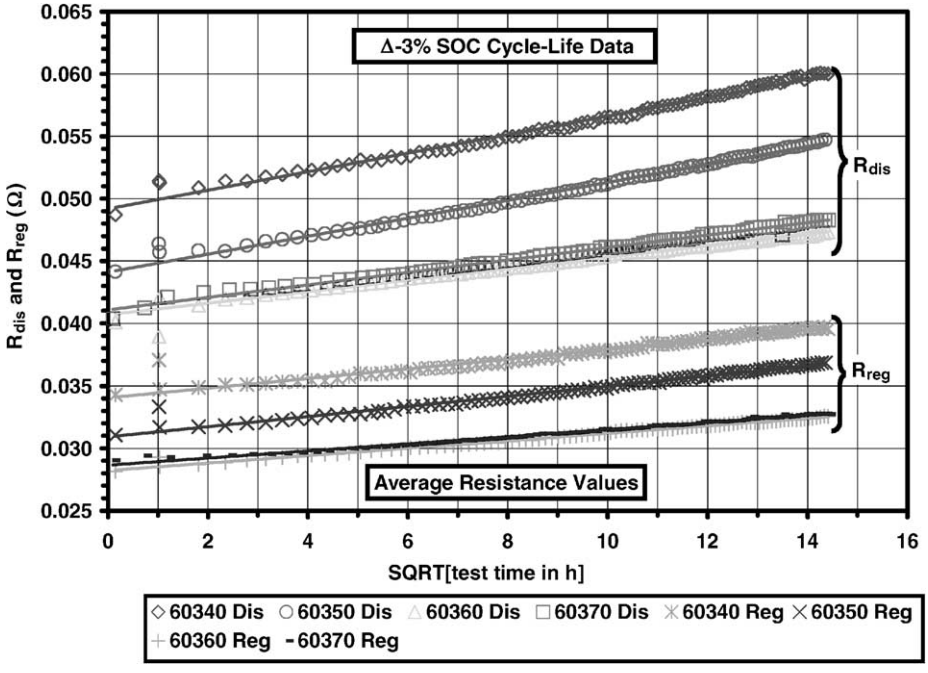

Fig. 10. Average of all INEEL cycle-life discharge and regen resistance data for the Δ3% cycle-life (60340, 60350, 60360 and 60370) tests as a function of the square-root of the test time.

for the calendar-life tests as previously discussed. It can also be observed in Fig. 10 that the discharge resistance increased faster than the regen resistance at each test temperature as the slopes of the discharge data are greater than the regen data. The data shown also do not correspond to a period of 4 weeks for the 40, 50 and 60 °C tests, or to a 2-week period for the 70 °C test. Due to instrumentation problems, the data collection was interrupted at the longer test times. However, the tests did continue for the full 4- or 2-week period. With regard to the plots showing the resistance as a function of the square-root of test time, other time-dependent fitting functions were used in attempts to correlate the data given in this figure [6]. The square-root of test time gave the best fit to the resistance as was also found to be the case for the calendar-life tests described above.

Fig. 11 displays the fits of the average R_{dis} to the square-root of test time (h), using an expanded y-axis scale, for the four test temperatures. The slopes of the best fit to this time-dependent function, as well as the time-equal-to-zero intercepts are given in the figure. The goodness of fit at each of the test temperatures, R^2, is also given. The slopes and the intercept values are generally seen to decrease with increasing temperature. The R^2 values are also quite good. The exception is the 70 °C data, which have a slope larger than the data at 60 °C. Similarly, in Fig. 12 the fits to R_{reg} for the average of all the cells are shown for the four test temperatures. Again, the fits are quite good. The general trend is the same as that observed for R_{dis} in that as the temperature is increased, the slopes and intercepts decrease. The exception is the 70 °C data. Also, note from Figs. 10–12 that the R_{dis} slopes and intercept values are larger than those for R_{reg} at the same test temperature. This means that the discharge resistance is increasing at a greater rate than the regen resistance at the same temperature. The discharge resistance at zero time is also larger than the zero time regen resistance. This type of analysis was done on each of the cycle-life test cells at the Δ3, Δ6, Δ9% SOC swing tests.

A functional form for the description of the test time, temperature, SOC and Δ% SOC dependence of the discharge and regen resistances was assumed to be essentially the same as given in Eq. (8) for the calendar-life tests:

$$R(t, T, \mathrm{SOC}, \Delta\%\,\mathrm{SOC})) = A(T, \mathrm{SOC}, \Delta\%\,\mathrm{SOC})t^{1/2} + B(T, \mathrm{SOC}, \Delta\%\,\mathrm{SOC}) \quad (8)$$

with the addition of the A and B functions being dependent on the Δ% SOC swing of the test (either Δ3, Δ6 or Δ9% SOC). $A(T, \mathrm{SOC}, \Delta\%\,\mathrm{SOC})$ and $B(T, \mathrm{SOC}, \Delta\%\,\mathrm{SOC})$ are assumed to be only functions of the temperature, the SOC and the Δ% SOC. For brevity, $A(T, \mathrm{SOC}, \Delta\%\,\mathrm{SOC})$ is simply referred too as A, and $B(T, \mathrm{SOC}, \Delta\%\,\mathrm{SOC})$ is referred too as B unless the SOC dependence is specifically discussed. Once the functions for A and B have been determined, a physical/chemical basis for the functional forms are attempted, using the fits to the discharge and regen resistances as a guide.

In Fig. 13, the R_{dis} and R_{reg} A parameters are plotted as the exponential of the inverse of the temperature (K), i.e. $A = a[\exp(b/T)]$ for each of the test cells (three at each test temperature). The variation in the actual test temperature, measured by a thermocouple mounted on the cell body, is shown. The best-fit fitting parameters are shown in the figure for both the discharge and regen $A(T)$ values. From the fits

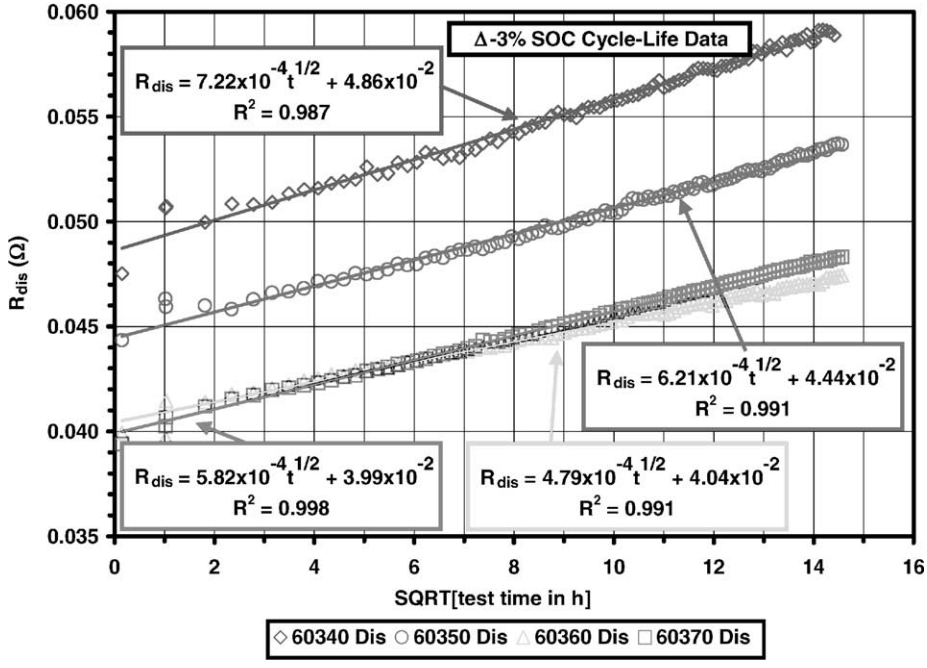

Fig. 11. Average of all INEEL cycle-life Δ3% (60340, 60350, 60360 and 60370) test discharge resistance data for ATD Gen 1 cells plotted as a function of the square-root of test time. The model fits to the relation: $R(t, T) = A(T)t^{1/2} + B(T)$ and the correlation coefficient (R^2) are given in the figure for each temperature.

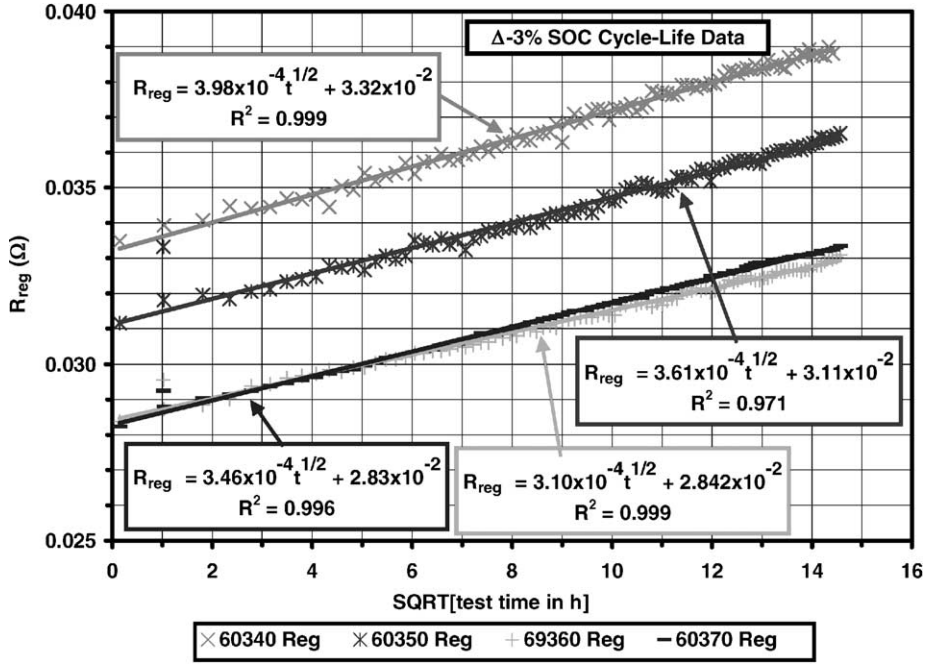

Fig. 12. Average of all INEEL cycle-life Δ3% (60340, 60350, 60360 and 60370) test regen resistance data for ATD Gen 1 cells plotted as a function of the square-root of test time. The model fits to the relation: $R(t,T) = A(T)t^{1/2} + B(T)$ and the correlation coefficient (R^2) are given in the figure for each temperature.

given in Fig. 13, the R_{dis} A parameter is seen to decrease at a slightly greater rate with increasing temperature than does the R_{reg} A parameter.

Fig. 14 presents a similar treatment of the temperature dependence of the B parameter as determined from each cell, also for the (60340, 60350, 60360 and 60370) test conditions. In this figure are plotted the R_{dis} and R_{reg} B parameters as a function of the exponential of the inverse of the temperature (K), i.e. $B = c[\exp(d/T)]$. The actual temperature of the cell is used in the plots. The fitting parameters and

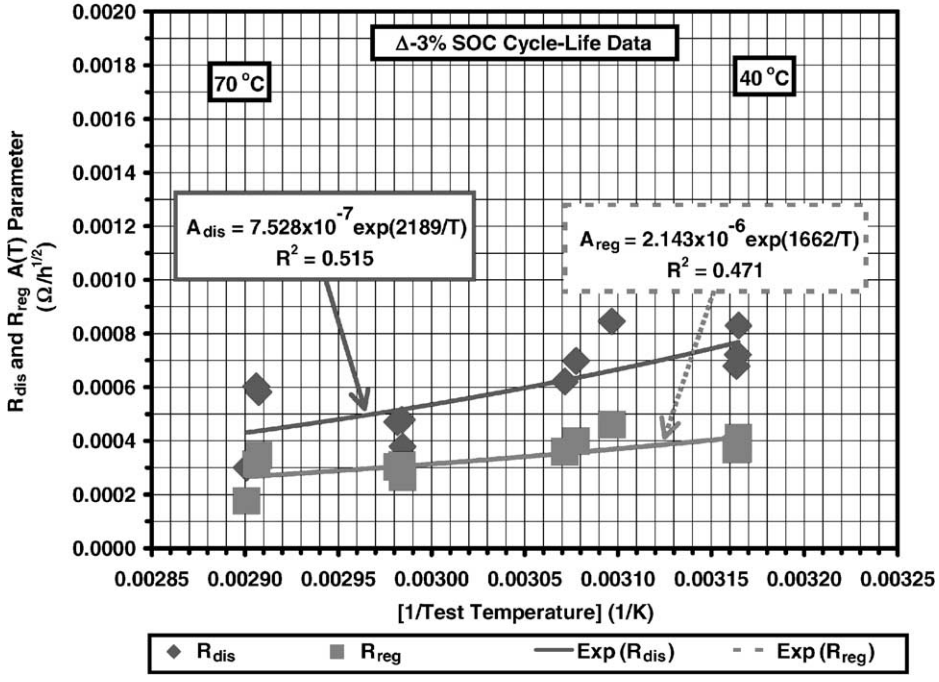

Fig. 13. $A(T)$ parameters from data fits to the cycle-life Δ3% (60340, 60350, 60360 and 60370) test to the model $R(t,T) = A(T)t^{1/2} + B(T)$ are shown as a function of the inverse test temperature (K). Fitting parameters to the model $A(T) = a[\exp(b/T)]$ are given for the discharge and regen resistance data.

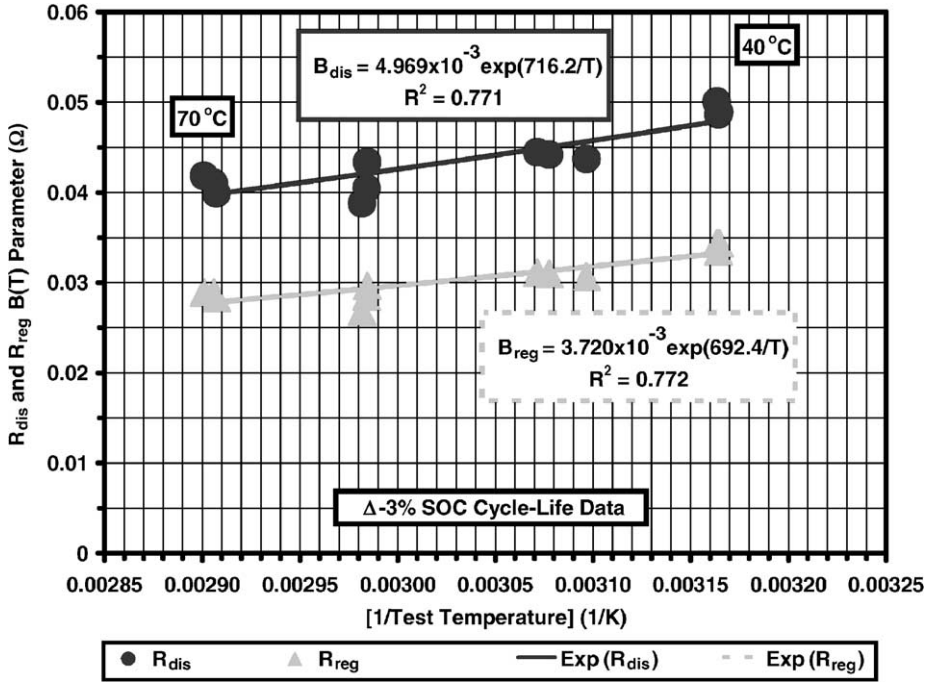

Fig. 14. $B(T)$ parameters from data fits to the cycle-life Δ3% (60340, 60350, 60360 and 60370) test to the model $R(t, T) = A(T)t^{1/2} + B(T)$ are shown as a function of the inverse test temperature (K). Fitting parameters to the model $B(T) = c[\exp(d/T)]$ are given for the discharge and regen resistance data.

R^2 are given in the figure. Hence, as was the case for the A parameter, the fits to the temperature dependence of the B parameter can be reasonably correlated by the exponential of the inverse temperature relation. Note that the scatter in the B parameter is much less than the scatter in the A parameter. As observed in this study, the A parameter determined from the square-root of test time data fits is very sensitive to the data. This occurs since subtle changes in the slopes of the data curves fitted to the square-root of the test time can significantly alter the A parameter. The B parameter, which represents the intercept of the square-root of test time fits, is less sensitive to the test data. From the fits given in Figs. 13 and 14, it can be seen that the R_{dis} A and B parameters decrease at a slightly greater rate with increasing temperature than do the R_{reg} A and B parameters.

Upon close examination of the values of A and B for the discharge and regen resistances shown in Figs. 13 and 14, it is not obvious that any one set of the parameters at a given temperature should be eliminated. Even though the discharge and regen resistance at 70 °C appear to indicate that a new mechanism is leading to a resistance increase of the cell during the test is occurring, all of the resistance values at all of the test temperatures were used in the model. The values for the discharge and regen activation energies and the pre-exponential coefficients determined from the data fits shown in Figs. 13 and 14 for the Δ3% SOC swing test are given in Tables 9 and 10. Note that the parameters a, b, c and d can be SOC-dependent as well as Δ% SOC-dependent, as explicitly shown in the following equation:

$$R(t, T, \mathrm{SOC}, \Delta\%\,\mathrm{SOC}) = a(\mathrm{SOC}, \Delta\%\,\mathrm{SOC}) \times \left\{\exp\left[\frac{b(\mathrm{SOC}, \Delta\%\,\mathrm{SOC})}{T}\right]\right\} t^{1/2} + c(\mathrm{SOC}, \Delta\%\,\mathrm{SOC}) \times \left\{\exp\left[\frac{d(\mathrm{SOC}, \Delta\%\,\mathrm{SOC})}{T}\right]\right\} \quad (9)$$

Table 9
Values of E_{act} at 60% SOC from analysis of cycle-life Δ3, Δ6 and Δ9% SOC test data using the relationship: $R(t, T) = A(T)t^{1/2} + B(T)$, where $A(T) = a[\exp(E_{act,A}/RT)]$ and $B(T) = c[\exp(E_{act,B}/RT)]$

Test condition	Activation energy ($E_{act,A}$, kJ/mol)	Activation energy ($E_{act,B}$, kJ/mol)
R_{dis} (60340, 60350, 60360 and 60370)	18.2 (4.35)	5.96 (1.42)
R_{reg} (60340, 60350, 60360 and 60370)	13.8 (3.30)	5.76 (1.38)
R_{dis} (60640, 60650, 60660 and 60670)	30.2 (7.23)	4.52 (1.08)
R_{reg} (60640, 60650, 60660 and 60670)	19.0 (4.53)	4.88 (1.17)
R_{dis} (60940, 60950, 60960 and 60970)	11.0 (2.63)	5.57 (1.33)
R_{reg} (60940, 60950, 60960 and 60970)	9.51 (2.27)	4.88 (1.17)

E_{act} are activation energies, and a and c are pre-exponential constants. The values given in parenthesis are in kcal/mol.

Table 10
Values of the pre-exponential constants a and c at 60% SOC from analysis of cycle-life test data analysis at Δ3, Δ6% and Δ9% SOC using the relationship: $R(t, T) = A(T)t^{1/2} + B(T)$, where $A(T) = a[\exp(E_{act,A}/RT)]$ and $B(T) = c[\exp(E_{act,B}/RT)]$

Test condition	Pre-exponential constant a (Ω per (day)$^{1/2}$)	Pre-exponential constant c ($\times 10^{-3}$ Ω)
R_{dis} (60340, 60350, 60360 and 60370)	7.53×10^{-7}	4.97
R_{reg} (60340, 60350, 60360 and 60370)	2.14×10^{-6}	3.72
R_{dis} (60640, 60650, 60660 and 60670)	1.14×10^{-8}	8.30
R_{reg} (60640, 60650, 60660 and 60670)	3.65×10^{-7}	5.22
R_{dis} (60940, 60950, 60960 and 60970)	1.21×10^{-5}	5.55
R_{reg} (60940, 60950, 60960 and 60970)	1.25×10^{-5}	5.08

Since only one SOC, 60%, was studied in this paper, the SOC dependence of the various parameters could not be determined. The dependence of the parameters on Δ% SOC is discussed later in this paper.

The comparison between the model predictions using Eq. (9) with the parameter values as given in Tables 9 and 10 and the experimental discharge and regen resistance data at the 60% SOC, Δ3% SOC charge swing cycle-life test are presented in Figs. 15 and 16. The model predictions are quite good for the 40 and 50 °C data. The model, however, would predict that the 60 °C resistance would be larger than the 70 °C resistance. Experimentally, this is not the case, as the 70 °C resistance values are slightly higher than the 60 °C values. Based on the model and the experimental data, new physical/chemical processes may be occurring at 60 and/or 70 °C that cause the resistance to not follow the general trend of a lower resistance the higher the temperature. Also shown in Figs. 15 and 16 are the model's prediction of the discharge and regen resistances for a test temperature of 25 °C. The ability to predict the discharge and regen resistances at temperatures other than ones studied experimentally is one of the main points in conducting this modeling effort. Unfortunately, there were no data acquired at 25 °C or other temperatures, which may be used to validate the model, particularly at the lower temperatures.

The discharge and regen resistances as a function of test time at temperature for the Δ6 and Δ9% SOC swing tests were analyzed in the same manner as was used for the Δ3% SOC swing test described earlier [6]. The best fit to the time dependence of the increase in the discharge and regen resistance was determined to be a square-root of time dependence as is shown in Eqs. (8) and (9). The A and B parameters were also found to be best represented by an Arrhenius-type of temperature function as shown in Eq. (9). The fits of the model as given in Eq. (9) used the resistance values at all of the test temperatures since it was not obvious

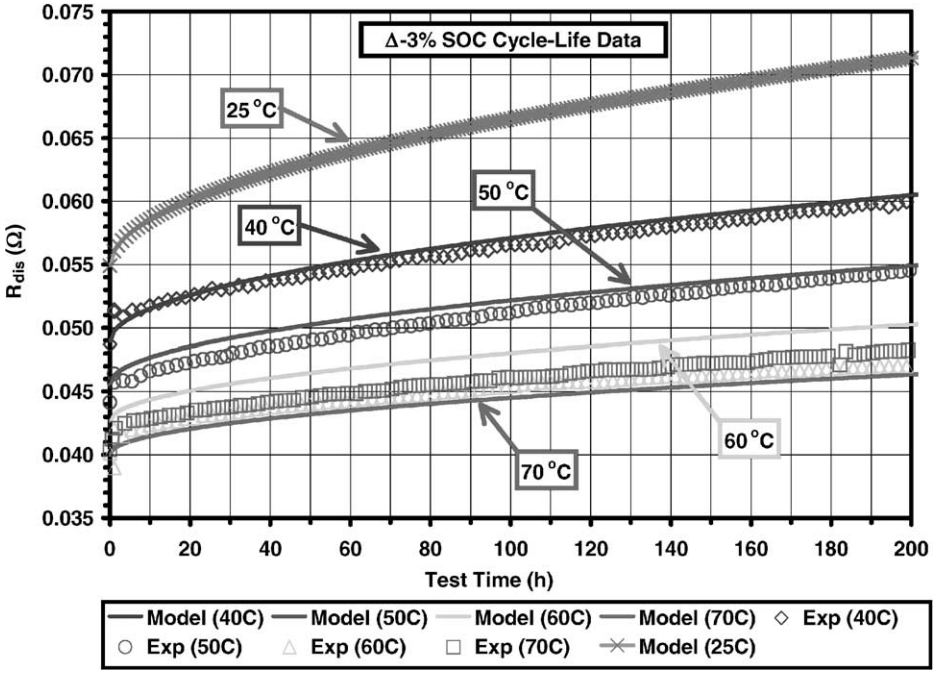

Fig. 15. Model predictions compared to cycle-life Δ3% discharge resistance data for ATD Gen 1 (60340, 60350, 60360 and 60370) tests. Model used the a, b, c and d parameters determined when all the test temperatures were used to fit the resistance data. The model prediction for a test temperature of 25 °C is also shown.

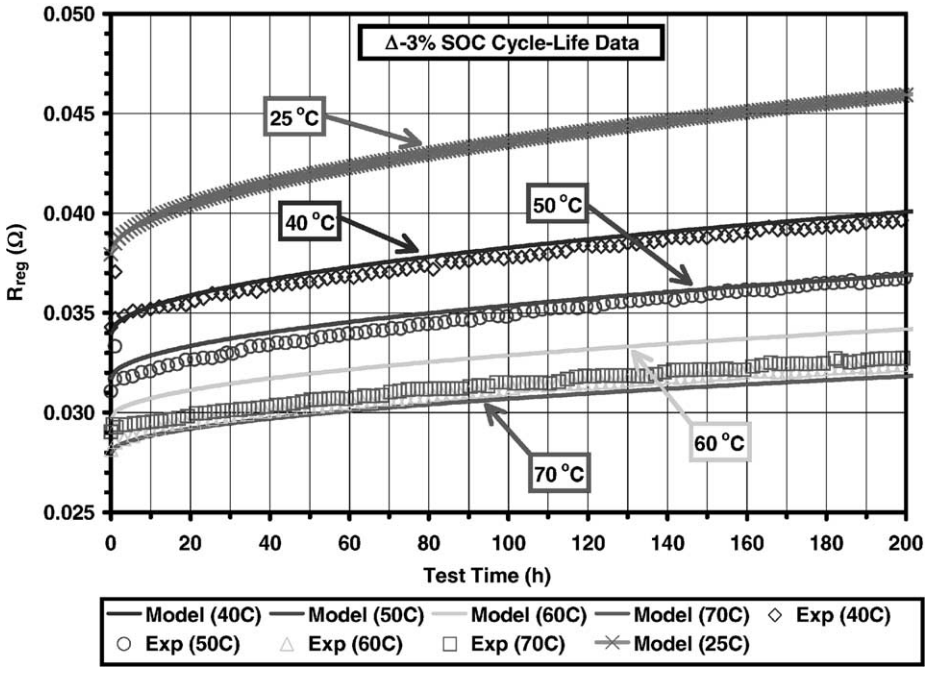

Fig. 16. Model predictions compared to cycle-life Δ3% regen resistance data for ATD Gen 1 (60340, 60350, 60360 and 60370) tests. Model used the *a*, *b*, *c* and *d* parameters determined when all the test temperatures were used to fit the resistance data. The model prediction for a test temperature of 25 °C is also shown.

which temperature data to eliminate from the plots of the $A(T)$ and $B(T)$ functions as a function of the inverse of the test temperature. The values of the discharge and regen activation energies and the pre-exponential coefficients determined from this analysis are given in Tables 9 and 10. The average of the experimental discharge and regen resistance and the model fits to the data using Eq. (9) with the parameter values given in Tables 9 and 10 are shown in Figs. 17 and 18 for the Δ6% SOC swing test, and in Figs. 19 and 20 for the Δ9% SOC swing test, respectively. Also shown are the model predictions for the discharge and regen resistance if the tests were conducted at 25 °C. The model fits are fairly good for the 40 and 50 °C discharge and regen resistance. The correlation to the 60 and 70 °C data is not as good, but the model predictions do bracket the resistance at these temperature values.

Upon examination of the activation energies presented in Table 9, several overall trends can be observed. The discharge activation energies for $E_{act,A}$ are greater than the corresponding regen $E_{act,A}$ activation energies. From Eq. (9), this indicates that the time rate of change of the discharge resistance is greater than the regen resistance. There appears to be no general trend for the $E_{act,A}$ activation energies, except to observe that the Δ6% SOC test values are higher than those for Δ3 and Δ9% test values. The $E_{act,B}$ activation energies are less than the $E_{act,A}$ activation energies. The $E_{act,B}$ activation energies are all about the same, probably within experimental error. At present, the authors know of no reason why the values given in Table 9 are what they are. They are about the correct order of magnitude for processes that may occur in a battery such as the various diffusion processes that appear to have activation energies of several tens of kJ/mol. The authors have been unable to find literature values for lithium-ion diffusion through the SEI layer present on the anode or cathode, or its diffusion in the anode or cathode materials for the electrode and electrolyte compositions used in the ATD Gen 1 cells. Similarly, the pre-exponential constant a shown in Table 10 is smaller for the discharge resistance than the regen resistance. The pre-exponential constant *c* for the discharge resistance is somewhat greater than the regen resistance value at each Δ% SOC test. Why this is so is not presently known.

In Eq. (9), it was assumed that the resistance was a function of the SOC of the cell at the beginning of the test pulse sequence, and that it was also a function of the SOC swing during the test, Δ% SOC. As only one SOC was tested, 60% SOC, the dependence of the resistance on this variable could not be determined. Attempts were made to find a consistent model of the parameters *a*, *b*, *c* and *d* as a function of the Δ% SOC of the test. No reasonably consistent model was found, nor were any insights into the Δ% SOC dependence found in the literature. Physical/chemical diagnostics being conducted on the test cells, as part of the ATD program, may provide future insight into the processes responsible for these model-determined values.

3.4. Comparison between calendar- and cycle-life tests

Upon comparison of the measured discharge and regen resistance values for the calendar-life tests conducted at 60

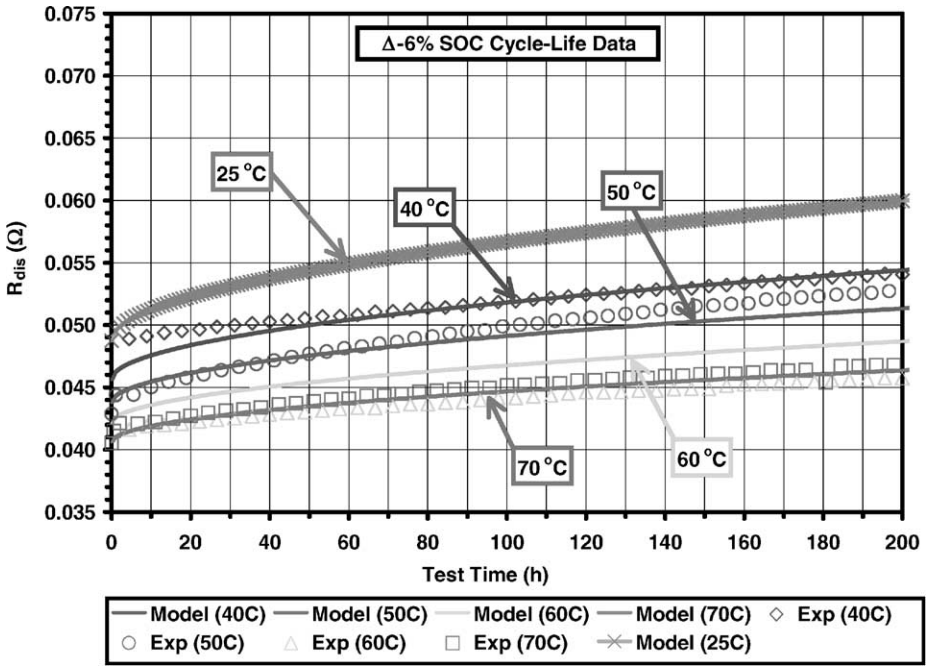

Fig. 17. Model predictions compared to cycle-life Δ6% discharge resistance data for ATD Gen 1 (60640, 60650, 60660 and 60670) tests. Model used the *a*, *b*, *c* and *d* parameters determined when all the test temperatures were used to fit the resistance data. The model prediction for a test temperature of 25 °C is also shown.

and 80% SOC with those measured at 60% SOC for the cycle-life tests (Figs. 5, 7–9 and 15–20), it can be seen that the both the discharge and regen resistance were greatest for the 80% SOC calendar-life test. The discharge and regen 60% SOC calendar-life test resistances were also greater than the 60% SOC cycle-life tests at Δ3, Δ6 and Δ9% at times less than 4 weeks. This observation is counter-intuitive as one would had expected that the cycle-life tests at Δ3, Δ6 and Δ9% SOC would have been more "abusive" on the cells resulting in a greater increase in their resistance with test

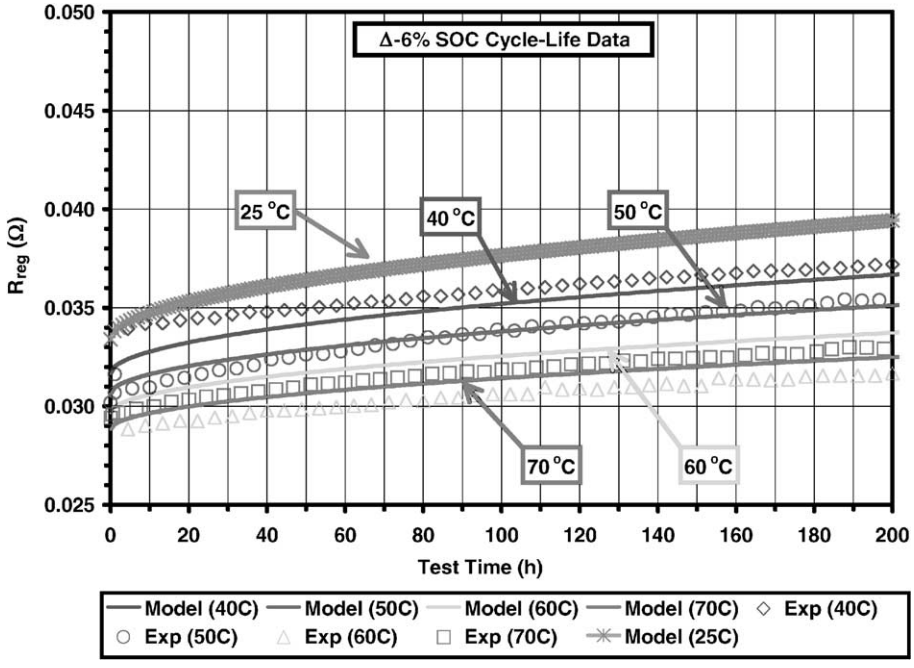

Fig. 18. Model predictions compared to cycle-life Δ6% regen resistance data for ATD Gen 1 (60640, 60650, 60660 and 60670) tests. Model used the *a*, *b*, *c* and *d* parameters determined when all the test temperatures were used to fit the resistance data. The model prediction for a test temperature of 25 °C is also shown.

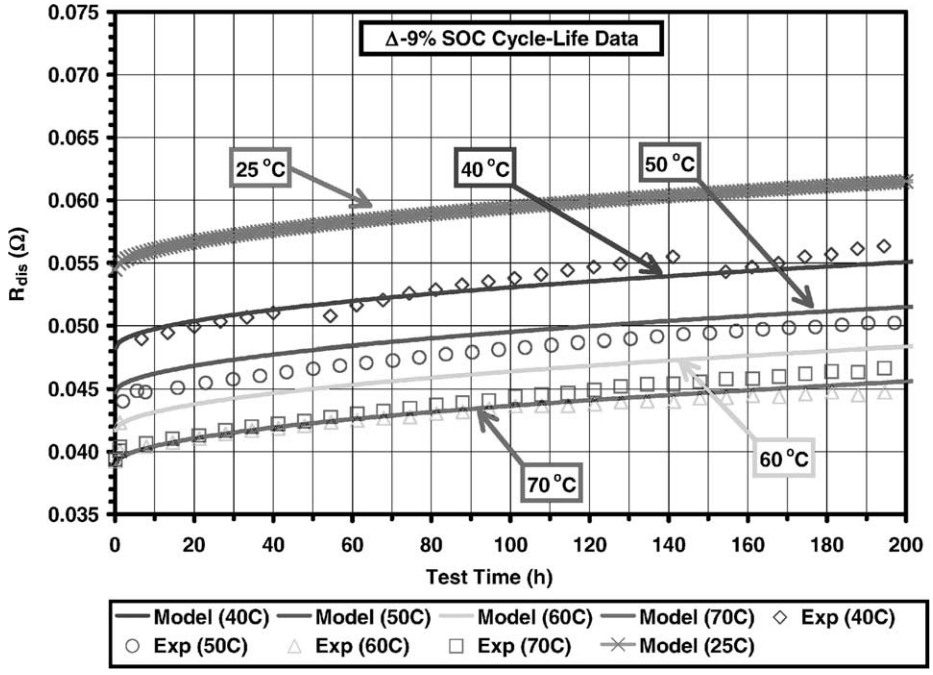

Fig. 19. Model predictions compared to cycle-life Δ9% discharge resistance data for ATD Gen 1 (60940, 60950, 60960 and 60970) tests. Model used the *a*, *b*, *c* and *d* parameters determined when all the test temperatures were used to fit the resistance data. The model prediction for a test temperature of 25 °C is also shown.

time. The calendar-life test had a percentage SOC swing of 1% (Table 1) on discharge and was conducted only once per day while the cycle-life tests were conducted almost continuously and had percentage SOC swings of 3, 6 and 9%. It was also initially thought that the order of the resistance increase for the cycle-life tests would have been Δ9% SOC > Δ6% SOC > Δ3% SOC because of the greater perturbation of the cell the greater the Δ% SOC swing. This

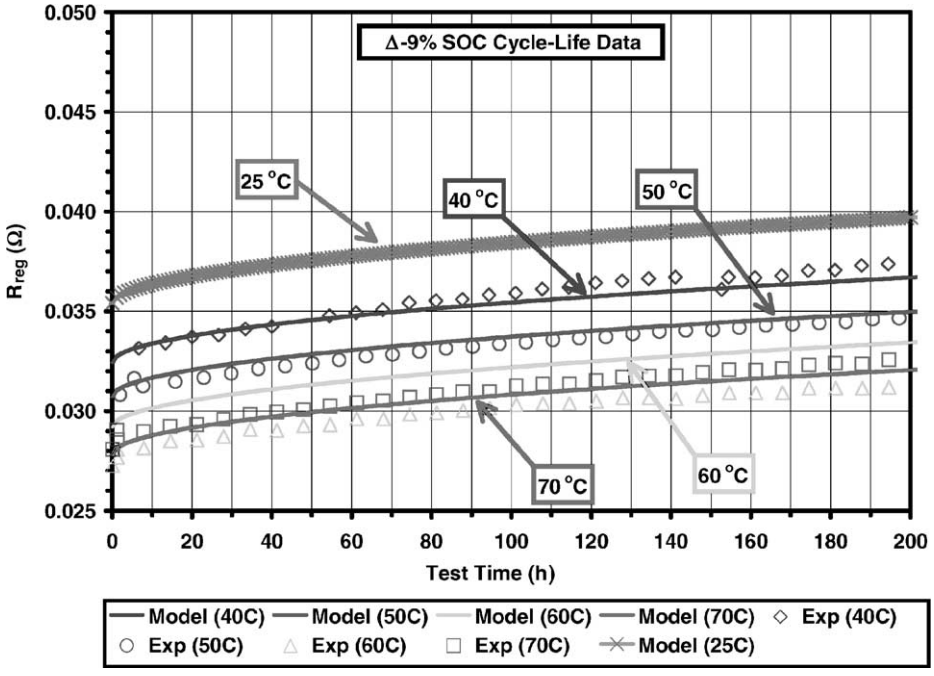

Fig. 20. Model predictions compared to cycle-life Δ9% regen resistance data for ATD Gen 1 (60940, 60950, 60960 and 60970) tests. Model used the *a*, *b*, *c* and *d* parameters determined when all the test temperatures were used to fit the resistance data. The model prediction for a test temperature of 25 °C is also shown.

also was not the case as the resistance at Δ3% was observed to increase to a greater extent that at Δ6 and Δ9% (at least for test times up to 200 h as shown in Figs. 15–20). It may well be that if the formation of the SEI layer is the primary cause of the resistance increase, that the rate of its formation is fairly slow such that the cycle-life tests are disrupting its formation on a rather continuous basis due to the discharging/charging cycles compared to when the cell is sitting for a longer period of time between discharging/charging cycles as in the calendar-life tests. That this may be the case is supported by the pre-exponential constant a for the tests as are given in Tables 8 and 10 for the various tests. It is observed in these tables that the pre-exponential constant a for the 60% SOC calendar-life test are greater than for the 60% SOC cycle-life tests. The time-rate-of-change of the discharge and regen resistance for the models given in Eqs. (7) and (9) is:

$$\frac{\mathrm{d}[R(t,T,\mathrm{SOC},\Delta\%\,\mathrm{SOC})]}{\mathrm{d}t} = a(\mathrm{SOC},\Delta\%\,\mathrm{SOC}) \times \left\{\frac{\exp[b(\mathrm{SOC},\Delta\%\,\mathrm{SOC})/T]}{2t^{1/2}}\right\} \quad (10)$$

This equation shows that the time-rate-of-change of the resistance not only depends on the a(SOC, Δ% SOC) pre-exponential constant, but also on the b(SOC, Δ% SOC) parameter that is related to the activation energy of the process. The activation energies, as shown in Tables 7 and 9, are greater for the cycle-life tests than for the calendar-life tests, so the actual rate of increase of the discharge and regen resistance depend on both the a(SOC, Δ% SOC) pre-exponential constant and also on the value of the term $\exp[E_{\mathrm{act}}(\mathrm{SOC}, \Delta\%\ \mathrm{SOC})/RT]$. This relation indicates that an increase in one parameter can be compensated for by a decrease in the other. Direct comparisons of the discharge and regen resistance for the 80 and 60% SOC calendar-life tests and the 60% SOC cycle-life tests as predicted using the model as given in Eqs. (7) and (9), and the fitting parameters given in Tables 5–10 for a test temperature of 25 °C are given in Figs. 20 and 21, respectively, for a time period of 365 days. Examining the discharge resistance for the (80C25) test, it can be seen that the it is the greatest at this test condition compared to any of the other tests. The discharge resistance for the (60C25) test condition is also greater than the all of the Δ% SOC cycle-life tests except for the Δ6% test whose resistance is predicted to becomes larger after ∼100 days. The Δ3% SOC cycle-life discharge resistance is greater than the Δ9% SOC tests over the entire time period shown in Fig. 21. The model predictions for the regen resistances at 25 °C (Fig. 22) for the various tests shows that the calendar-life test caused the resistance to increase to a greater extent then any of the Δ% SOC tests. At the longer test times (∼>15 days), the regen resistance for the cycle-life tests is in the order Δ6% *SOC* > Δ3% SOC > Δ9% SOC. At present, we have no explanation for these trends as they are not what would have been expected before the actual testing of the batteries. Thus, the exact nature of the test, and the SOC at which the test is conducted (and the Δ% SOC swing for the cycle-life tests) all have a major influence on the aging of the batteries and the change in the discharge and regen resistance during a given test.

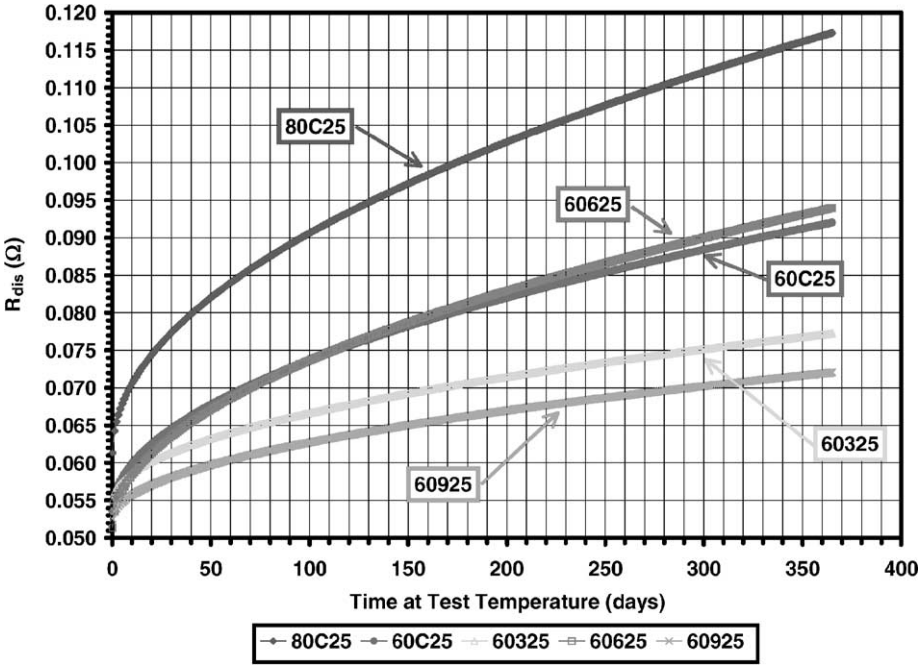

Fig. 21. Model predictions for a time period of 365 days for calendar- and cycle-life discharge resistance for ATD Gen 1 cells at different test conditions.

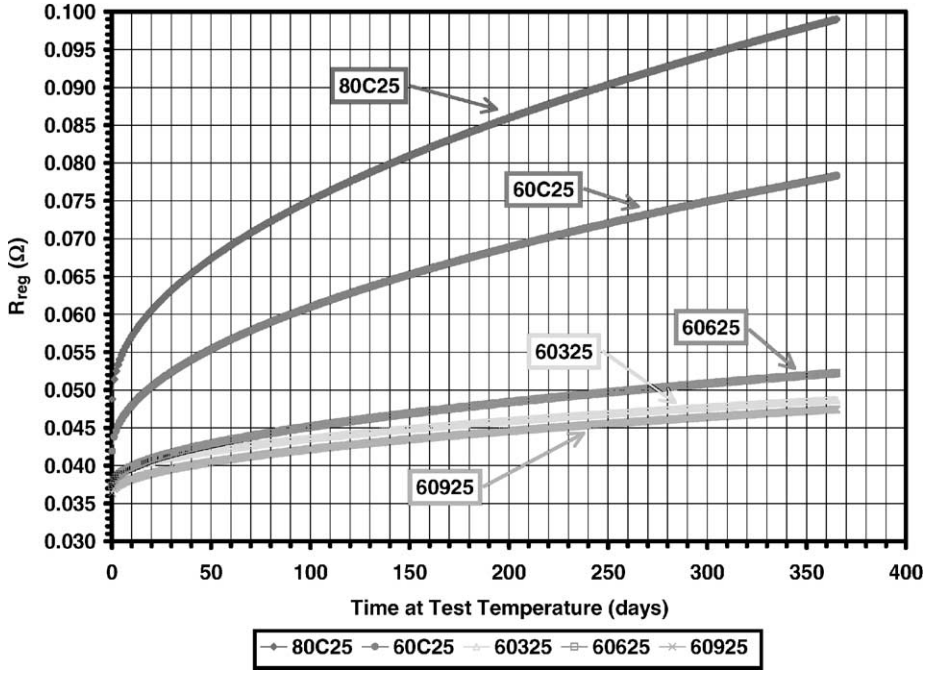

Fig. 22. Model predictions for a time period of 365 days for calendar- and cycle-life regen resistance for ATD Gen 1 cells at different test conditions.

4. Conclusions

This paper presented the test results pertaining to a group of ATD program Gen 1 lithium-ion batteries. The cells underwent a number of electrical performance tests to determine their electrochemical performance at 25 °C. Special calendar- and cycle-life tests were also conducted at elevated temperatures of 40, 50, 60 and 70 °C for specified periods of time.

One of the specific tests for which the data are presented and discussed was a special calendar-life test conducted once per day for specified periods of time, depending on the test temperature. The calendar-life test was conducted at 60 and 80% SOC. During the calendar-life test, the discharge resistance was determined from the discharge portion of the test using Ohm's law. The regen resistance was determined from the regen portion of the test also using Ohm's law.

General observations derived from this study are the following.

1. Both the discharge and regen resistances have a non-linear increase with respect to time at test temperature.
2. The discharge resistance is greater than the regen resistance at all test temperatures of 40, 50, 60 and 70 °C.
3. For both the discharge and regen resistance, generally the higher the test temperature, the lower the resistance.
4. The 70 °C discharge and regen resistance data at 80% SOC do not follow the general trend of the rest of the data in that the resistance at this temperature is slightly greater than at 60 °C. At 60% SOC, the discharge and regen resistance data indicate a process is occurring that causes the 60 °C resistance to be slightly greater or comparable to those at 50 °C. At this SOC, the 70 °C may also have been influenced. These observations appear to indicate that a new physical/chemical process is occurring that causes the resistance to increase in an anomalous manner. They also indicate that the SOC at which the test was conducted may influence the temperature at which the onset of these new processes occurs. The exact nature of these processes is not presently known.
5. Both the discharge and regen resistances at a given temperature are greater at 80% SOC than they are at 60% SOC.
6. There are also differences in the rate of increase of the resistances in that the 80% SOC resistance increases with time at test temperature faster than at 60% SOC.

A life model was developed to account for the time, temperature and SOC of the batteries during the calendar-life test. The of modeling effort led to the relationship for the discharge and regen resistance having the form: $R(t, T, \mathrm{SOC}) = a(\mathrm{SOC})\{\exp[b(\mathrm{SOC})/T]\}t^{1/2} + c(\mathrm{SOC})\{\exp[d(\mathrm{SOC})/T]\}$. The square-root of time dependence can be accounted for by either a one-dimensional diffusion-type of mechanism, presumably of the lithium-ions or by a parabolic growth mechanism for the growth of a thin-film SEI layer on the anode and/or cathode. The temperature dependence of the resistances have the form of an Arrhenius-like process that could be related to the diffusion of the lithium-ions or to chemical processes related to the formation of the SEI surface film. The function $R(t, T, \mathrm{SOC})$

was then be used to correlate the discharge and regen resistance data and to predict what the resistances would be at different test times at particular test conditions and at different test temperatures.

The other specific test for which the data are presented and discussed in this paper was a special cycle-life test conducted for a 4-week period at test temperatures of 40, 50 and 60 °C, and for a 2-week period at 70 °C. This test, consisting of three specified discharge and charge protocols, was designed to have a Δ3, Δ6 or Δ9% cumulative SOC swings during the discharge portion of the test cycle.

The results of the cycle-life testing indicate that both the discharge and regen resistance increased in a non-linear manner as a function of the test time at each Δ% SOC test. The magnitude of the discharge and regen resistances depended on the temperature and Δ% SOC at which the test was conducted. General observations derived from this study are the following.

1. Both the discharge and regen resistances have a non-linear increase with respect to time at test temperature, i.e. as the number of test cycles increased, the discharge and regen resistance increased also.
2. For a given Δ% SOC test, the discharge resistances are greater than the regen resistance at all of the test temperatures of 40, 50, 60 and 70 °C.
3. For both the discharge and regen resistances, generally the higher the test temperature, the lower the resistance.
4. The 70 °C discharge and regen resistance data do not always follow the general trend of the rest of the data in that the resistance at this temperature are slightly greater than at 60 °C. This observation appears to indicate that new physical/chemical processes are occurring that causes the resistance to increase. The exact nature of these processes is not presently known.
5. At each of the four test temperatures, the magnitude of the discharge and regen resistance was in the following order for the first 200 h test period: Δ3% SOC > Δ9% SOC > Δ6% SOC. At longer test times, the model predicts that the relative order of the discharge and regen resistance at a given Δ% SOC test would be Δ6% SOC > Δ3% SOC > Δ9% SOC. No explanation is currently known for this observation. There are research groups within the ATD program currently conducting physical/chemical studies on the test cells that may offer insight into this observation.

A life model was developed to account for the time, temperature, SOC and Δ% SOC of the batteries during the cycle-life test. The functional form of the model is given by: $R(t, T, \mathrm{SOC}, \Delta\%\ \mathrm{SOC}) = a(\mathrm{SOC}, \Delta\%\ \mathrm{SOC})\{\exp[b(\mathrm{SOC}, \Delta\%\ \mathrm{SOC})/T]\}t^{1/2} + c(\mathrm{SOC}, \Delta\%\ \mathrm{SOC})\{\exp[d(\mathrm{SOC}, \Delta\%\ \mathrm{SOC})/T]\}$. This model is essentially the same as was used to model the calendar-life discharge and regen resistances. The values determined for the functions a, b, c and d were different than those determined for the calendar-life tests. Due to the lack of testing at SOC values other than 60% SOC, the exact form of the SOC dependence could not be determined from the cycle-life data. Attempts were made to find a consistent correlation of the observed resistance changes with the Δ% SOC of the tests, but no model based on physical/chemical processes was found.

Acknowledgements

This work was performed under the auspices of the US Department of Energy, Assistant Secretary for Energy Efficiency and Renewable Energy (EE), specifically the Office of Advanced Automotive Technologies (OATT), under DOE Idaho Operations Office, Contract DE-AC07-00ID13727.

References

[1] FY-1999 progress report for the advanced technology development program, US Department of Energy, Office of Advanced Automotive Technologies, 1000 Independence Avenue SW, Washington, DC 20585-0121, March 2000.
[2] USABC Electric Vehicle Battery Test Procedures Manual, Revision 2, DOE/ID-10479, January 1996.
[3] PNGV Battery Test Manual, Revision 2, DOE/ID-10597, August 1999 (A new version of this manual has been released: PNGV Battery Manual, Revision 3, DOE/ID-10597, February 2001).
[4] PNGV Test Plan for ATD 18650 Gen 1 Lithium-Ion Cells, Revision 4, EHV-TP-103, December 1999.
[5] R.B. Wright, C.G. Motloch, Calendar-life studies of advanced technology development program Gen 1 lithium-ion batteries, Report DOE/ID-10844, March 2001.
[6] R.B. Wright, C.G. Motloch, Cycle-life studies of advanced technology development program Gen 1 lithium-ion batteries, Report DOE/ID-10845, April 2001.
[7] I. Bloom, B.W. Cole, J.J. Sohn, S.A. Jones, E.G. Polzin, V.S. Battaglia, G.L. Henriksen, C.G. Motloch, R.A. Richardson, T. Unkelhaeuser, D. Ingersol, H.L. Case, J. Power Sources 101 (2001) 238.
[8] D. Zhang, B.S. Haran, A. Durairajan, R.E. White, Y. Podrazhansky, B.N. Popov, J. Power Sources 91 (2000) 122.
[9] H. Wang, Y.-I. Jang, B. Huang, D.R. Sadoway, Y.-M. Chiang, J. Electrochem. Soc. 146 (1999) 473.
[10] M.G.S.R. Thomas, P.G. Bruce, J.B. Goodenough, J. Electrochem. Soc. 132 (1985) 1521.
[11] P. Arora, R.E. White, M. Doyle, J. Electrochem. Soc. 145 (1998) 3647.
[12] S.R. Narayanan, D.H. Shen, S. Surampudi, A.I. Attia, G. Halpert, J. Electrochem. Soc. 140 (7) (1993) 12.
[13] K. Ozawa, Solid State Ionics 69 (1994) 212.
[14] S. Megahed, B.S. Scrosati, J. Power Sources 51 (1994) 79.
[15] G. Nagasubramanian, FY-1999 progress report for the advanced technology development program, March 2000, p. 42.
[16] J. Baker, P. Shaw, G. Nagasubramanian, D. Doughty, in: Proceedings of the Electrochemical Society, Vol. 99-25, New Jersey, 2000, p. 664.
[17] D. Guyomard, J.M. Tarascon, J. Power Sources 54 (1995) 92.
[18] D. Aurbach, B. Markovsky, I. Weissman, E. Levi, I. Ein-Eli, Electrochem. Acta 45 (1999) 67.
[19] B. Markovsky, M.D. Mikhail, D. Aurbach, Electrochem. Acta 16/17 (1998) 2287.
[20] N. Birks, G.H. Meier, Introduction to High Temperature Oxidation of Metals, Arnold, London, 1983.
[21] P. Kofstad, High-Temperature Oxidation of Metals, Wiley, New York, 1966.

[22] K. Hauffe, Oxidation of Metals, Plenum Press, New York, 1965.
[23] G.E. Blomgren, J. Power Sources 81/82 (1999) 112.
[24] C. Kittel, Introduction to Solid State Physics, 4th Edition, Wiley, New York, 1971.
[25] W. Jost, Diffusion in Solids, Liquids and Gases, 3rd Printing, Addendum, Academic Press, New York, 1960.
[26] J. Crank, The Mathematics of Diffusion, 2nd Edition, Clarendon Press, Oxford, 1975.
[27] Per Kofstad, Non-stoichiometry, diffusion and electrical conductivity, in: Binary Metal Oxides, Wiley, New York, 1972.
[28] J.P. Fellner, G.J. Loeber, S.S. Sandhu, J. Power Sources 81/82 (1999) 867.